

An Internally-Consistent Database for Oxygen Isotope Fractionation Between Minerals

Alice Vho^{1*}, Pierre Lanari ¹ and Daniela Rubatto^{1,2}

¹Institute of Geological Sciences, University of Bern, Baltzerstrasse 1-3, Bern CH-3012, Switzerland; ²Institut de Sciences de la Terre, University of Lausanne, Lausanne CH-1015, Switzerland

*Corresponding author. Present address: Institute of Geological Sciences, University of Bern, Baltzerstrasse 1-3, Bern CH-3012, Switzerland. Tel: +41 31 631 4738. E-mail: alice.vho@geo.unibe.ch

Received October 30, 2018; Accepted December 31, 2019

ABSTRACT

The knowledge of the fractionation behaviour between phases in isotopic equilibrium and its evolution with temperature is fundamental to assist the petrological interpretation of measured oxygen isotope compositions. We report a comprehensive and updated internally consistent database for oxygen isotope fractionation. Internal consistency is of particular importance for applications of oxygen isotope fractionation that consider mineral assemblages rather than individual mineral couples. The database DBO_{OXYGEN} is constructed from a large dataset of published experimental, semi-empirical and natural data, which were weighted according to type. It includes fractionation factors for 153 major and accessory mineral phases and a pure H₂O fluid phase in the temperature range of 0–900°C, with application recommended for temperatures of 200–900°C. Multiple primary data for each mineral couple were discretized and fitted to a model fractionation function. Consistency between the models for each mineral couple was achieved by simultaneous least square regression. Minimum absolute uncertainties based on the spread of the available data were calculated for each fractionation factor using a Monte Carlo sampling technique. The accuracy of the derived database is assessed by comparisons with previous oxygen isotope fractionation calculations based on selected mineral/mineral couples. This database provides an updated internally consistent tool for geochemical modelling based on a large set of primary data and including uncertainties. For an effective use of the database for thermometry and uncertainty calculation we provide a MATLAB[®]-based software THERMOX. The new database supports isotopic modelling in a thermodynamic framework to predict the evolution of δ¹⁸O in minerals during metamorphism.

Key words: oxygen isotopes; δ¹⁸O; internal consistency; thermometry; petrological modelling

INTRODUCTION

Stable isotopes are important tools for a wide range of applications in Earth Sciences as the isotopic composition of minerals can record their physical and chemical conditions of equilibration. Oxygen isotope fractionation between two cogenetic minerals is, for example, temperature-dependent and has been intensively used as mineral thermometer (e.g. [Bottinga & Javoy, 1973](#); [Clayton, 1981](#); [Zheng, 1993a](#)). Additionally, the oxygen isotope composition of co-existing phases is a prime tool for reconstructing fluid–rock interaction and evaluating mineral equilibration (e.g. [Valley, 1986, 2001](#); [Eiler *et al.*, 1992, 1993](#); [Kohn, 1993](#); [Valley & Graham, 1996](#);

[Baumgartner & Valley, 2001](#); [Page *et al.*, 2014](#); [Rubatto & Angiboust, 2015](#)). Such applications require the knowledge of the fractionation behaviour between two mineral phases as well as the possible evolution with temperature. Over the past decades, efforts have been directed towards the determination of fractionation factors between minerals or minerals and fluids. Pioneer works were mostly based on experimental data on isotope exchange between minerals and water ([Clayton, 1961](#); [O’Neil & Taylor, 1967](#); [Clayton *et al.*, 1972](#); [Matsuhisa *et al.*, 1979](#); [Matthews *et al.*, 1983a](#)), whereas mineral/mineral couples were often derived by combining these calibration data.

Phase equilibrium modelling of metamorphic rocks has evolved to a point where mineral assemblages are being considered, rather than individual mineral couples (see Lanari & Duesterhoeft, 2019 for a review). A step forward can also be anticipated for oxygen thermometry and isotopic tracing, provided that the fractionation factors between several minerals can be combined in a similar way to that done for the thermodynamic data of minerals (e.g. Berman, 1988; Holland & Powell, 1998) or aqueous species (Miron *et al.*, 2016, 2017). Ideally, the achievement of internal consistency can be defined as the optimal satisfaction of the simultaneous constraints imposed by all the data. The internal consistency of a database can be formulated as a list of increasingly stringent conditions (Engi, 1992), including: (1) compatibility with theoretical definitions and reference values; (2) representation of all of the listed data, in the sense of 'best compromise' with all of the available data considered simultaneously; and (3) compatibility with all underlying data within stated uncertainties.

For oxygen isotope fractionation, early works combining experimental data on different minerals resulted in self-consistent compilations (e.g. Bottinga & Javoy, 1975; Chiba *et al.*, 1989; Matthews, 1994), each of them involving typically less than 10 minerals. The more recent compilation by Chacko *et al.* (2001) based on carbonate exchange experiments includes 15 minerals. A more considerable effort is needed for critical assessment of a larger pool of primary data and for their transformation into an internally consistent dataset. A second category of database for oxygen isotope fractionation factors is based on semi-empirical calculations such as the theory of bond strength models (Garlick, 1966; Schütze, 1980). For instance, the work of Zheng (1991, 1992, 1993a, 1993b, 1993c, 1996, 1999) resulted in a large database of semi-empirical data and offering partial compatibility within individual mineral groups (Zheng, 1999). In that approach, the change of reference mineral from quartz (Zheng, 1991, 1992, 1993a, 1993b) to calcite (Zheng, 1996, 1999) does not guarantee consistency between the different groups.

Internal consistency is a fundamental criterion for advanced applications of oxygen isotope fractionation that consider mineral assemblages rather than individual mineral couples. However, internal consistency is difficult to achieve as there are several reasons, such as experimental errors, inadequate theory or assumptions, or poor measurements, that may cause minor or major discrepancies between different calibrations (May & Murray, 2001). In this regard, combination of natural, experimental, theoretical and semi-empirical data could be used to overcome the limits of each method. This paper presents a large and internally consistent database for oxygen isotope fractionation between minerals. The first section describes how existing oxygen isotope fractionation data were selected, weighted and processed. We offer a different approach than other

databases that provide calculations based on single calibration chosen by the user (see AlphaDelta by G. Beaudoin & P. Therrien available at http://www2.ggl.ulaval.ca/cgi-bin/alphadelta/alphadelta_4alpha.cgi). Our approach considers simultaneously a large number of mineral couples and maximises the consistency of the oxygen isotope fractionation among all of them. It enables calculations to be done using phase couples for which no direct data is available, and it is directed to modelling rock systems where the $^{18}\text{O}/^{16}\text{O}$ composition of every phase is required to be in equilibrium with every other phase, in an internally consistent manner. The significance of the results and their uncertainties is discussed in detail and possible applications in metamorphic petrology are shown. The internally consistent database DBOXYGEN version 2.0.3 contains fractionation factors for 153 minerals and a pure water fluid phase based on a large compilation of literature data (Table 1). We also present the MATLAB[®]-based software THERMOX that uses this database for thermometry and uncertainty calculation. The database, supporting information, software solutions and further updates are available for download at <http://oxygen.petrochronology.org/>.

Methods for estimating oxygen isotope fractionation between phases

Controlled laboratory experiments using natural or synthetic phases are the most commonly used method for estimating oxygen isotope fractionation between mineral and fluid phases. The fractionation factors are obtained by interpolating the experimental data points along the temperature range [T_{min} , T_{max}] of the experiments. However, the method of equilibrium exchange requires temperatures where isotopic exchange is sufficiently rapid to reach equilibrium in a reasonable amount of time, typically $T > 500^\circ\text{C}$. The success of this type of experiments can be limited by small exchange amounts and failure to attain complete isotopic equilibrium (O'Neil, 1986; Chacko *et al.*, 2001). Significant advances in experimental techniques are represented for instance by (1) the development of the three isotope exchange method to estimate equilibrium fractionation from partially exchanged samples (e.g. Matsuhisa *et al.*, 1978; Matthews *et al.*, 1983a, 1983b, 1983c) and (2) the introduction of piston-cylinder high-pressure exchange experiments that allow mineral-water and mineral-calcite exchange to occur much faster than in the previously used conventional 1–2 kbar hydrothermal apparatus (e.g. Clayton *et al.*, 1975; Matsuhisa *et al.*, 1978; Matthews *et al.*, 1983a, 1983b, 1983c). The compilation by Chacko *et al.* (2001) revisited in detail experiments published before 2001.

Beside experimental calibrations, the statistical mechanical theory of isotope fractionation developed by Bigeleisen & Mayer (1947) and Urey (1947) was used by Bottinga & Javoy (1973) to derive an interpretive

Table 1: Mineral phases and phase end-members in the database. *A*, *B* and *C* are the calculated fractionation factors (as reported in Eq. 4) for quartz/mineral. Fractionation factors for water are given as quartz/water. Uncertainties (at 2σ) are reported in brackets. References for the primary data evaluated for the calculation are reported. References in *italics* were not used for the final optimization (see text and [Supplementary Data 1](#) for details). For the chemical formula of each phase, reference is made to the original source of the data

Phases	A (2σ)	B (2σ)	C (2σ)	References: (*) Quartz/Phase; (**) Phase/H ₂ O; (***) Calcite/Phase
Water	4.11 (0.11)	-3.33 (0.61)	0.00 (0.15)	(*) 1, 2, 3, 4, 5, 6, 7, 8, 9, 10, 11, 12, 86, 87, 88, 89
Carbonates				
Ankerite	0.41 (0.01)	-0.29 (0.01)	0.00 (0.00)	(*, **, ***) 17; 91
Aragonite	0.28 (0.16)	1.23 (0.02)	0.00 (0.01)	(*) 17; (**) 17; 92; 93; 94
Azurite	2.83 (0.03)	-9.43 (0.00)	0.00 (0.02)	(**) 108
Calcite	0.39 (0.26)	0.15 (0.15)	0.00 (0.08)	(*) 3; 10; 17; 19; 90; (**) 5; 13; 14; 15; 16; 17; 109; 110
Cerussite	0.68 (0.00)	0.01 (0.00)	0.00 (0.01)	(*) 17; (**) 17; 18
Dolomite	0.24 (0.21)	-0.21 (0.00)	0.00 (0.00)	(*) 17; 91; (**) 15; 17; 21; 91; 95; 96; 97; 98; (***) 15; 91; 99; 100
Magnesite	0.38 (0.02)	-0.21 (0.03)	0.00 (0.00)	(*, **) 17
Malachite	2.71 (0.00)	-8.42 (0.01)	0.00 (0.30)	(**) 108
Norsethite	0.49 (0.07)	0.14 (0.01)	0.00 (0.00)	(*, ***) 91; (**) 52; 91
Otavite	0.64 (0.16)	-0.23 (0.01)	0.00 (0.02)	(*) 17; (**) 14; 17
Rhodochrosite	0.56 (0.02)	-0.80 (0.05)	0.00 (0.04)	(*) 17; (**) 17; 101
Siderite	0.30 (0.05)	-0.09 (0.01)	0.00 (0.01)	(*) 17; (**) 1; 17; 53; 54
Smithsonite	-0.06 (0.05)	0.27 (0.01)	0.00 (0.01)	(*, **) 17
Strontianite	0.82 (0.09)	-0.21 (0.20)	0.00 (0.24)	(*) 17; (**) 16; 17
Witherite	0.78 (0.11)	0.33 (0.04)	0.00 (0.01)	(*) 17; (**) 14; 16; 17
Feldspar group				
Albite	0.33 (0.00)	0.53 (0.02)	0.00 (0.13)	(*) 7; 12; 23; 24; (**) 2; 7; 9; 12; 25; (***) 12; 23; 26; 90
Anorthite	0.71 (0.00)	1.13 (0.64)	0.00 (0.07)	(*) 7; 12; 23; 24; 28; (**) 2; 7; 9; 12; 25; (***) 12; 23; 26; 90
K-Feldspar	0.20 (0.00)	1.08 (0.01)	0.00 (0.03)	(*) 12; 28; (**) 9; 12; 25; (***) 12; 26
Garnet Group				
Almandine	1.29 (0.01)	1.98 (0.01)	0.00 (0.36)	(*) 12; 29; (**) 9; 12; (***) 12
Andradite	1.17 (0.03)	2.35 (0.01)	0.00 (0.12)	(*) 12; (**) 9; 12; (***) 12; 26
Grossular	1.37 (0.01)	1.91 (0.02)	0.00 (0.35)	(*) 12; 27; 29; 30; (**) 9; 12; 30; (***) 12; 26; 30; 31
Pyrope	1.18 (0.01)	2.39 (0.00)	0.00 (0.24)	(*, ***) 12; (**) 9; 12
Spessartine	1.29 (0.01)	2.04 (0.03)	0.00 (0.18)	(*) 12; 32; (**) 9; 12; 32; (***) 12
Melanite	1.15 (0.01)	2.02 (0.00)	0.00 (0.01)	(**) 9
Uvarovite	1.13 (0.02)	2.46 (0.07)	0.00 (0.16)	(*, ***) 12 (***) 9; 12;
Epidote group				
Allanite	1.68 (0.04)	1.83 (0.01)	0.00 (0.01)	(**) 9
Epidote	0.57 (0.00)	2.23 (0.03)	0.00 (0.95)	(*) 30; 33; 34; 35; (**) 9; 35; (***) 35
Piemontite	1.21 (0.01)	2.02 (0.00)	0.00 (0.06)	(**) 9
Zoisite	0.81 (0.00)	1.82 (0.91)	0.00 (0.98)	(*) 30; 35; (**) 9; 35; 37; (***) 30; 35
Amphibole group				
Actinolite	0.81 (0.02)	2.11 (0.01)	0.00 (0.14)	(*, **, ***) 35
Anthophyllite	0.81 (0.01)	2.12 (0.02)	0.00 (0.16)	(*, **, ***) 35
Cumingtonite	0.86 (0.01)	1.99 (0.01)	0.00 (0.13)	(*, ***) 35; (**) 9; 35
Edenite	1.91 (0.02)	0.95 (0.01)	0.00 (0.00)	(**) 9; (***) 26
Gedrite	1.04 (0.01)	2.21 (0.09)	0.00 (0.05)	(*, ***) 35; (**) 9; 35
Glaucophane	0.73 (0.00)	1.92 (0.02)	0.00 (0.29)	(*) 28; 35; 38; (**) 9; 35; (***) 26
Grunerite	0.80 (0.01)	2.04 (0.06)	0.00 (0.09)	(*, **, ***) 35
Hornblende	0.90 (0.00)	2.37 (0.11)	0.00 (0.21)	(*) 28; 35; (**) 9; 35; (***) 26; 35
Katophorite	2.58 (0.01)	-0.31 (0.02)	0.00 (0.01)	(**) 9
Pargasite	1.13 (0.00)	2.38 (0.03)	0.00 (0.21)	(*) 35; (**) 9; 35; (***) 26; 35
Richterite	-0.58 (0.02)	3.89 (0.04)	0.00 (0.03)	(**) 9
Riebeckite	0.63 (0.00)	2.01 (0.05)	0.00 (0.16)	(*, **, ***) 35
Taramite	1.65 (0.00)	1.15 (0.03)	0.00 (0.01)	(**) 9
Tremolite	0.81 (0.02)	2.15 (0.04)	0.00 (0.16)	(*) 35; (**) 9; 35; (***) 26; 35
Tschemmakite	1.42 (0.00)	1.48 (0.01)	0.00 (0.00)	(**) 9; (***) 26
Chlorite group				
Chamosite	0.69 (0.02)	1.78 (0.06)	0.00 (0.00)	(*, **, ***) 35
Chlorite	0.47 (0.00)	3.12 (0.00)	0.00 (0.04)	(*) 39; (**) 9; 40
Clinochlore	0.76 (0.00)	2.17 (0.05)	0.00 (0.18)	(*, **, ***) 35
Thuringite	0.88 (0.02)	2.31 (0.07)	0.00 (0.19)	(*, **, ***) 35
Mica group				
Annite	0.92 (0.00)	2.29 (0.03)	0.00 (0.23)	(*, ***) 35; (**) 9; 35
Biotite	0.90 (0.00)	2.67 (0.09)	0.00 (0.49)	(*) 41; 28; 35; (**) 9; 35; (***) 26; 35

(continued)

Table 1: Continued

Phases	A (2σ)	B (2σ)	C (2σ)	References: (*) Quartz/Phase; (**) Phase/H ₂ O; (***) Calcite/Phase
Glauconite	0.84 (0.03)	1.82 (0.01)	0.00 (0.01)	(*, ***) 35; (**) 9; 35
Lepidolite	0.61 (0.01)	1.69 (0.02)	0.00 (0.07)	(*, ***) 35; (**) 9; 35
Margarite	0.51 (0.01)	2.06 (0.01)	0.00 (0.29)	(*) 35; (**) 9; 35; (***) 26; 35
Muscovite	0.85 (0.01)	1.06 (0.03)	0.00 (0.25)	(*) 2; 19; 27; 28; 34; 35; 42; (**) 2; 9; 35; 43; (***) 19; 26; 35
Paragonite	0.62 (0.00)	1.55 (0.01)	0.00 (0.08)	(*) 35; (**) 9; 35; 43; (***) 26; 35
Phengite	0.55 (0.02)	1.68 (0.08)	0.00 (0.13)	(*) 35; (**) 9; 35; (***) 26; 35
F-phlogopite	2.13 (0.02)	0.00 (0.03)	0.00 (0.45)	(*) 27; (***) 19; 44
Phlogopite	1.17 (0.00)	1.79 (0.08)	0.00 (0.49)	(*) 27; 35; (**) 9; 35; (***) 19; 26; 35
Pyroxene group				
Acmite	0.53 (0.00)	1.29 (0.00)	0.00 (0.00)	(*, ***) 12; (**) 9; 12
Diopside	1.03 (0.02)	1.74 (0.03)	0.00 (0.36)	(*) 12; 23; 24; (**) 9; 12; (***) 12; 23; 26
Hedenbergite	0.86 (0.01)	2.16 (0.02)	0.00 (0.15)	(*, ***) 12; (**) 9; 12
Jadeite	0.63 (0.01)	1.09 (0.06)	0.00 (0.28)	(*) 12; 24; 30; (**) 9; 12; 30; (***) 12; 26; 30
Enstatite	0.76 (0.01)	2.23 (0.14)	0.00 (0.69)	(*, **) 9; 12; (***) 12
Ferrosilite	0.72 (0.01)	2.15 (0.08)	0.00 (0.92)	(*, **) 12; (**) 9; 12
Olivine group				
Fayalite	1.20 (0.00)	3.03 (0.56)	0.00 (0.88)	(*, **) 9; 12; (***) 12
Forsterite	1.50 (0.02)	2.84 (1.04)	0.00 (0.21)	(*) 9; 12; 23; (**) 9; 12; (***) 12; 23; 26; 46
Tephroite	1.21 (0.01)	3.01 (0.01)	0.00 (0.46)	(*, **) 12
Zeolite group				
Analcime	0.47 (0.00)	-0.01 (0.00)	0.00 (0.01)	(**) 55
Stilbite	0.54 (0.00)	-0.56 (0.02)	0.00 (0.02)	(**) 47
Wairakite	2.06 (0.02)	0.59 (0.00)	0.00 (0.02)	(**) 48
Al₂SiO₅ group				
Andalusite	0.33 (0.00)	1.72 (0.01)	0.00 (0.37)	(*) 22; 49; (**) 9; 22; (***) 22; 26
Kyanite	0.40 (0.00)	1.87 (0.01)	0.00 (0.23)	(*) 22; 49; (**) 9; 22; (***) 22; 26; 50
Sillimanite	0.06 (0.00)	1.91 (0.03)	0.00 (0.68)	(*) 22; 49; (**) 9; 22; (***) 22; 26
Topaz	0.51 (0.01)	1.42 (0.00)	0.00 (0.04)	(*, **, ***) 35
Spinel group				
Hercynite	3.05 (0.02)	4.81 (0.00)	0.00 (0.94)	(*, **, ***) 51
Spinel	3.25 (0.03)	4.85 (0.03)	0.00 (0.96)	(*, **, ***) 51
Ulvospinel	2.46 (0.01)	4.27 (0.04)	0.00 (0.73)	(*, **, ***) 51
Ilmenite group				
Geikelite	2.49 (0.00)	4.32 (0.09)	0.00 (0.85)	(*, **, ***) 51
Ilmenite	2.37 (0.01)	4.17 (0.03)	0.00 (0.69)	(*, **, ***) 51
Humite group				
Chondrodite	1.14 (0.01)	2.59 (0.02)	0.00 (0.29)	(*, **, ***) 35
Clinohumite	1.08 (0.00)	2.48 (0.06)	0.00 (0.19)	(*, **, ***) 35
Humite	1.07 (0.01)	2.55 (0.04)	0.00 (0.30)	(*, **, ***) 35
Norbergite	1.26 (0.00)	2.92 (0.03)	0.00 (0.37)	(*, **, ***) 35
Serpentine group				
Amesite	0.72 (0.01)	2.44 (0.07)	0.00 (0.31)	(*, ***) 35; (**) 9; 35
Chrysotile	2.43 (0.01)	1.33 (0.06)	0.00 (0.01)	(**) 9
Lizardite	0.84 (0.00)	1.96 (0.02)	0.00 (0.11)	(*, **, ***) 35
Serpentine	0.73 (0.02)	2.35 (0.02)	0.00 (0.41)	(*, ***) 35; (**) 35; 40; 56
Clay mineral group				
Illite	0.74 (0.03)	0.91 (0.14)	0.00 (0.04)	(*) 35; 57; (**) 9; 35; 58; (***) 35
Kaolinite	0.51 (0.13)	0.96 (0.00)	0.00 (0.00)	(*, ***) 35; (**) 9; 35; 59; 60; 61
Pyrophyllite	0.06 (0.01)	0.67 (0.02)	0.00 (0.00)	(*, **, ***) 35
Smectite	1.54 (0.01)	-3.42 (0.02)	0.00 (0.03)	(**) 9; 58; 62
Talc	0.28 (0.01)	1.89 (0.05)	0.00 (0.27)	(*) 35; (**) 9; 35; (***) 26; 35
Titanite group				
Malayaite	0.90 (0.00)	2.40 (0.03)	0.00 (0.26)	(*, **, ***) 12
Titanite	1.05 (0.01)	2.41 (0.05)	0.00 (0.85)	(*) 12; 26; 63; (**) 9; 12; (***) 12; 26

(continued)

Table 1: Continued

Phases	A (2σ)	B (2σ)	C (2σ)	References: (*) Quartz/Phase; (**) Phase/H ₂ O; (***) Calcite/Phase
Feldspathoid group				
Leucite	0.37 (0.01)	1.13 (0.00)	0.00 (0.00)	(*, **, ***) 12
Nepheline	0.61 (0.01)	1.64 (0.02)	0.00 (0.04)	(*, **, ***) 12
Pyroxenoid group				
Pectolite	0.65 (0.00)	1.77 (0.03)	0.00 (0.08)	(*, **, ***) 35
Rhodonite	0.95 (0.01)	2.40 (0.00)	0.00 (0.28)	(*, **, ***) 12
Phenacite group				
Phenacite	1.51 (0.02)	3.29 (0.01)	0.00 (0.48)	(*, **, ***) 12
Willemite	1.04 (0.00)	2.56 (0.03)	0.00 (0.32)	(*, **, ***) 12
Zircon group				
Thorite	1.14 (0.01)	2.83 (0.01)	0.00 (0.38)	(*, **, ***) 12
Zircon	1.56 (0.03)	1.23 (0.16)	0.00 (0.27)	(*) 12; 29; 64; 104; (**) 9; 12; 64
Other silicates				
Axinite	0.41 (0.02)	1.47 (0.02)	0.00 (0.01)	(*, **, ***) 35
Beryl	0.79 (0.01)	1.99 (0.01)	0.00 (0.13)	(*, **, ***) 12
Chloritoid	0.77 (0.00)	2.00 (0.03)	0.00 (0.10)	(*, **, ***) 35
Cordierite	0.66 (0.00)	1.58 (0.03)	0.00 (0.02)	(*, **) 12; (***) 12; 26
Datolite	0.18 (0.01)	1.02 (0.03)	0.00 (0.01)	(*, **, ***) 35
Gehlenite	3.54 (0.00)	0.00 (0.01)	0.00 (0.01)	(*, ***) 19; 27
Ilvaite	1.52 (0.00)	3.23 (0.00)	0.00 (0.49)	(*, **, ***) 35
Lawsonite	1.93 (0.00)	0.21 (0.12)	0.00 (0.02)	(*) 65
Prehnite	0.65 (0.08)	1.30 (0.00)	0.00 (0.04)	(*, **, ***) 35
Staurolite	0.46 (0.00)	2.25 (0.00)	0.00 (0.39)	(*) 35; 42; (**) 9; 35; (***) 26; 35
Tourmaline	0.43 (0.01)	1.35 (0.04)	0.00 (0.21)	(*) 35; 105; 106; (**, ***) 35
Wollastonite	1.36 (0.01)	1.52 (0.03)	0.00 (0.35)	(*) 12; 24; (**) 9; 12; (***) 12; 26
Vesuvianite	1.39 (0.01)	2.91 (0.04)	0.00 (0.30)	(*, ***) 35; (**) 9; 35
Oxides				
Cassiterite	1.06 (0.01)	3.30 (0.06)	0.00 (0.77)	(*, **) 51; 70; (***) 51
Cerianite	2.81 (0.01)	4.41 (0.16)	0.00 (0.63)	(*, **, ***) 51
Chromite	2.69 (0.01)	4.50 (0.04)	0.00 (0.80)	(*, **, ***) 51
Corundum	2.98 (0.01)	5.54 (0.16)	0.00 (0.18)	(*, **, ***) 51
Franklinite	2.62 (0.01)	4.31 (0.09)	0.00 (0.72)	(*, **, ***) 51
Hematite	1.32 (0.67)	5.86 (0.06)	0.00 (0.62)	(*, ***) 51 (**) 51; 66; 67; 68
Jacobsite	2.18 (0.00)	4.03 (0.07)	0.00 (0.66)	(*, **, ***) 51
Magnesiocromite	2.84 (0.03)	4.67 (0.08)	0.00 (0.86)	(*, **, ***) 51
Magnesioferrite	2.26 (0.04)	4.13 (0.00)	0.00 (0.69)	(*, **, ***) 51
Magnetite	2.34 (0.03)	4.00 (2.37)	0.00 (0.43)	(*) 23; 24; 28; 41; 51; (**) 1; 2; 51; (***) 23; 51
Perovskite	6.86 (0.04)	0.00 (0.01)	0.00 (0.02)	(*) 27; (***) 69
Plattnerite	1.26 (0.00)	2.73 (0.04)	0.00 (0.28)	(*, **, ***) 51
Pyrolusite	1.32 (0.01)	3.07 (0.03)	0.00 (0.41)	(*, **, ***) 51
Rutile	1.50 (0.04)	3.68 (0.29)	0.00 (0.94)	(*) 27; 30; 34; 51; 71; 72; 73; (**) 51; 71; 73; 113; (***) 27; 30; 51
Thorianite	2.75 (0.00)	4.50 (0.01)	0.00 (0.84)	(*, **, ***) 51
Uraninite	2.66 (0.02)	4.52 (0.02)	0.00 (0.88)	(*, ***) 51; (**) 51; 112
Wolframite	0.73 (0.01)	3.08 (0.12)	0.00 (0.86)	(*, **) 51; 70
Hydroxides				
Akaganeite	-2.76 (0.01)	9.48 (0.07)	0.00 (0.02)	(**) 66
Brucite	1.75 (0.04)	3.62 (0.02)	0.00 (0.57)	(*, ***) 75; (**) 58; 75; 76; 77
Bayerite	1.00 (0.00)	2.51 (0.05)	0.00 (0.29)	(*, **, ***) 75
Boehmite	1.88 (0.00)	3.74 (0.01)	0.00 (0.74)	(*, **, ***) 75
Diaspore	1.89 (0.01)	3.78 (0.04)	0.00 (0.64)	(*, **, ***) 75
Geothite	1.73 (0.03)	3.04 (0.00)	0.00 (0.22)	(*, ***) 75; (**) 66; 68; 75; 78; 111
Gibbsite	1.17 (0.12)	1.83 (0.01)	0.00 (0.02)	(*, ***) 75; (**) 75; 74; 78
Lepidocrocite	1.68 (0.02)	3.32 (0.02)	0.00 (0.43)	(*, **, ***) 75
Limonite	0.83 (0.01)	2.04 (0.00)	0.00 (0.16)	(*, **, ***) 75
Nordstrandite	1.01 (0.02)	2.24 (0.00)	0.00 (0.18)	(*, **, ***) 75
Pyrochroite	1.48 (0.01)	3.20 (0.02)	0.00 (0.46)	(*, **, ***) 75
Spertiniite	1.33 (0.00)	2.97 (0.11)	0.00 (0.30)	(*, **, ***) 75
Phosphates				
Apatite	1.64 (0.02)	1.14 (0.00)	0.00 (0.05)	(*) 27; 81; 107; (***) 27; 80; 81; 107
Monazite	0.85 (0.01)	1.33 (0.08)	0.00 (0.44)	(*) 81; 84; 85

(continued)

Table 1: Continued

Phases	A (2σ)	B (2σ)	C (2σ)	References: (*) Quartz/Phase; (**) Phase/H ₂ O; (***) Calcite/Phase
Xenotime	-0.13 (0.00)	-0.38 (0.01)	0.00 (0.00)	(*, **, ***) 81
Sulfates				
Alunite	-0.01 (0.00)	1.00 (0.00)	0.00 (0.00)	(**) 82
Anglesite	0.70 (0.02)	0.10 (0.01)	0.00 (0.00)	(*, **) 17
Anhydrite	-0.06 (0.00)	-0.05 (0.00)	0.00 (0.00)	(*) 17; (**) 17; 102; 103
Barite	0.52 (0.00)	0.72 (0.01)	0.00 (0.05)	(*, ***) 17; (**) 17; 83
Salts				
Portlandite	1.73 (0.00)	3.53 (0.09)	0.00 (0.47)	(*, **, ***) 75

References: (1) Becker & Clayton (1976); (2) Bottinga & Javoy (1973); (3) Clayton *et al.* (1972); (4) Friedman & O'Neil (1977); (5) Hu & Clayton (2003); (6) Kawabe (1978); (7) Matsuhisa *et al.* (1979); (8) Matthews & Beckinsale (1979); (9) Richter & Hoernes (1988); (10) Sharp & Kirschner (1994); (11) Zhang *et al.* (1989); (12) Zheng (1993a); (13) Epstein *et al.* (1953); (14) Kim & O'Neil (1997); (15) Northrop & Clayton (1966); (16) O'Neil *et al.* (1969); (17) Zheng (1999); (18) Melchiorre *et al.* (2001); (19) Chacko *et al.* (1996); (20) O'Neil & Clayton (1964); (21) Matthews & Katz (1977); (22) Zheng (1993c); (23) Chiba *et al.* (1989); (24) Matthews *et al.* (1983a); (25) O'Neil & Taylor (1967); (26) Hoffbauer *et al.* (1994); (27) Chacko *et al.* (2001); (28) Javoy *et al.* (1970); (29) Valley *et al.* (2003); (30) Matthews (1994); (31) Rosenbaum & Matthey (1995); (32) Lichtenstein & Hoernes (1992); (33) Kohn & Valley (1998b); (34) Matthews & Schliestedt (1984); (35) Zheng (1993b); (36) Cole *et al.* (1987); (37) Matthews *et al.* (1983c); (38) Kohn & Valley (1998c); (39) Lacroix & Vennemann (2015); (40) Wenner & Taylor (1971); (41) Bottinga & Javoy (1975); (42) Kohn & Valley (1998a); (43) O'Neil & Taylor (1969); (44) Fortier *et al.* (1994); (45) Kohn (1993); (46) Zheng *et al.* (1994); (47) Feng & Savin (1993); (48) Noto & Kusakabe (1997); (49) Sharp (1995); (50) Tennie *et al.* (1998); (51) Zheng (1991); (52) Böttcher (2000); (53) Carothers *et al.* (1988); (54) Zhang *et al.* (2001); (55) Karlsson & Clayton (1990); (56) Früh-Green *et al.* (1996); (57) Eslinger & Savin (1973); (58) Savin & Lee (1988); (59) Sheppard & Gilg (1996); (60) Eslinger (1971); (61) Kulla (1978); (62) Escande *et al.* (1984); (63) King *et al.* (2001); (64) Krylov *et al.* (2002); (65) Taylor Jr & Coleman (1968); (66) Bao & Koch (1999); (67) Clayton & Epstein (1961); (68) Yapp (1990); (69) Gautason *et al.* (1993); (70) Zhang *et al.* (1994); (71) Addy and Garlick (1974); (72) Agrinier (1991); (73) Matthews *et al.* (1979); (74) Bird *et al.* (1994); (75) Zheng (1998); (76) Saccoccia *et al.* (1998); (77) Xu and Zheng (1999); (78) Müller (1995); (79) Vitali *et al.* (2000); (80) Fortier & Lüttge (1995); (81) Zheng (1996); (82) Stoffregen *et al.* (1994); (83) Kusakabe & Robinson (1977); (84) Breecker & Sharp (2007); (85) Rubatto *et al.* (2014); (86) Shiro & Sakai (1972); (87) Kita *et al.* (1985); (88) Leclerc & Labeyrie (1987); (89) Brandriss *et al.* (1998); (90) Clayton *et al.* (1989); (91) Zheng & Böttcher (2016); (92) Kim *et al.* (2007); (93) Patterson *et al.* (1993); (94) Grossman & Ku (1986); (95) Vasconcelos *et al.* (2005); (96) Fritz & Smith (1970); (97) Schmidt *et al.* (2005); (98) Horita (2014); (99) O'Neil & Epstein (1966); (100) Sheppard & Schwarz (1970); (101) Kim *et al.* (2009); (102) Lloyd (1968); (103) Chiba *et al.* (1981); (104) Trail *et al.* (2009); (105) Kotzer *et al.* (1993); (106) Matthews *et al.* (2003); (107) Zheng (2016); (108) Melchiorre *et al.* (2000); (109) Coplen (2007); (110) Horita & Clayton (2007); (111) Yapp (1987); (112) Fayek & Kyser (2000); (113) Bird *et al.* (1993).

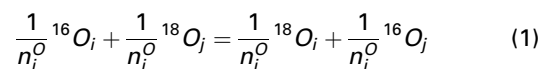
equation for oxygen isotope fractionation. Kieffer (1982) used fundamental theory and lattice dynamics, whereas Schütze (1980), Richter & Hoernes (1988), Zheng (1993a), Hoffbauer *et al.* (1994) based their incremental calculations on semi-empirical bond-strength models after the seminal studies of Taylor & Epstein (1962) and Garlick (1966). More recently, Hayles *et al.* (2018) proposed a calibration based on statistical thermodynamics and density functional theory combined with a semi-empirical approach to model liquid water (Bottinga & Javoy, 1973; Richter & Hoernes, 1988; Hoffbauer *et al.*, 1994). Compilations of semi-empirical calibrations by the increment method of fractionation factors provide fractionation data for a large variety of minerals over a wide temperature range. However, they are not fundamental harmonic oscillator or lattice dynamic calculations, but rather simplified model calculations based on bonding properties and, as such, their validity remains limited.

The third approach to obtain fractionation factors is the investigation of natural samples (e.g. Bottinga & Javoy, 1975; Kohn & Valley, 1998a; Valley, 2003; Lacroix & Vennemann, 2015). The analysed mineral phases are assumed to have coexisted in equilibrium at a temperature that is determined with an independent thermometer and the isotopic compositions to be preserved during cooling. In general, experiments and semi-empirical calculations have been favoured, largely due to the recognition of widespread diffusional resetting of isotope in natural samples, making many natural rocks inappropriate for retrieving equilibrium fractionation factors (e.g. Giletti, 1986; Eiler *et al.*, 1992, 1993; Kohn & Valley, 1998a; Valley, 2001).

THEORETICAL BACKGROUND

Oxygen isotope fractionation

The equilibrium fractionation of oxygen isotopes between two minerals can be described in terms of a chemical reaction in which isotopes are exchanged, in some ways analogous to the cation partitioning between minerals (e.g. Clayton, 1981; Chacko *et al.*, 2001). Assuming ideal mixing of isotopes ¹⁸O and ¹⁶O among the different oxygen sites in two phases *i* and *j* with number of atoms of oxygen n_i^O and n_j^O respectively, partitioning of the molar abundances ¹⁶O_{*i*}, ¹⁸O_{*i*}, ¹⁶O_{*j*} and ¹⁸O_{*j*} can be described by the reaction



The equilibrium constant *K* is

$$K = {}^{18}\text{O} / \frac{{}^{16}\text{O}}{{}^{18}\text{O} / {}^{16}\text{O}} \quad (2)$$

If the reaction is written such that one mole of ¹⁸O and ¹⁶O are exchanged between the two minerals, *K* is equal to the oxygen isotope fractionation factor between the two minerals $\alpha_{i,j}$:

$$K = {}^{18}\text{O} / \frac{{}^{16}\text{O}}{{}^{18}\text{O} / {}^{16}\text{O}} = \alpha_{i-j} \quad (3)$$

In most cases, temperature is assumed to be the main variable controlling isotope fractionation behaviour of mineral and water phases (e.g. Bigeleisen & Mayer, 1947; Urey, 1947; Joy & Libby, 1960; Stern *et al.*, 1968; Bottinga & Javoy, 1973; Clayton *et al.*, 1975;

Clayton, 1981; Hamann *et al.*, 1984; Criss, 1999). The equation that can reproduce most of the available calibrations describing the stable isotope fractionation function between two phases is a second-order polynomial of $10^3/T$:

$$1000 \cdot \ln \alpha_{i-j} = \left(\frac{A_{i-j} \cdot 10^6}{T^2} + \frac{B_{i-j} \cdot 10^3}{T} + C_{i-j} \right) \quad (4)$$

where α_{i-j} is the isotopic fractionation factor between i and j , T the temperature in K and A , B and C characteristic polynomial parameters describing the partitioning between phases i and j (units: $\text{‰} \cdot \text{K}^2$, $\text{‰} \cdot \text{K}$ and ‰ respectively). Despite the fact that different types of polynomial equations have been used in previous studies to describe the dependence of $1000 \cdot \ln \alpha_{i-j}$ from T (e.g. Clayton & Kieffer, 1991; Chacko & Deines, 2008; Hayles *et al.*, 2018), in this study we adopt the most widely-used expression (Eq. 4). As dictated by theory, isotopic fractionations between any two phases must approach 0‰ ($\alpha_{i-j} = 1$) as temperature goes to infinity. Therefore, the C term of Equation (4) was forced to be 0. The uncertainty assigned to this value is discussed below. Values of α_{i-j} are normally very close to unity, typically $1.00X$, and the fractionation is often considered to be equal to X (i.e. if $\alpha_{i-j} = 1.003$ then $\Delta^{18}\text{O}_{i-j} = 3\text{‰}$) (Sharp, 2017). In natural studies, it is common to report the isotopic composition of a phase as $\delta^{18}\text{O}$, representing the value of the ratio of stable isotope ^{18}O and ^{16}O expressed as a per mil deviation from a standard (‰), and the difference in isotopic composition between two phases as $\Delta^{18}\text{O}_{i-j}$. This value approximates well the quantity expressed as $1000 \cdot \ln \alpha_{i-j}$ when the individual values of $\delta^{18}\text{O}_i$ and $\delta^{18}\text{O}_j$ as well as $\Delta^{18}\text{O}_{i-j}$ are less than $\sim 10\text{‰}$ (Sharp, 2017). Such an approximation can be expressed as:

$$\Delta^{18}\text{O}_{i-j} = \delta^{18}\text{O}_i - \delta^{18}\text{O}_j \approx 1000 \cdot \ln \alpha_{i-j} \quad (5)$$

This approximation demands caution in the application of the equation at low temperatures ($< 200^\circ\text{C}$) where oxygen isotope fractionation between phases can be larger than 10‰ .

If the fractionation parameters between two couples $i-j$ and $i-k$ are known, parameters for the combined couple $k-j$ can be obtained from the algebraic sum

$$\begin{aligned} 1000 \cdot \ln \alpha_{i-k} &= 1000 \cdot \ln \alpha_{i-j} - 1000 \cdot \ln \alpha_{k-j} = \\ &= (A_{i-j} - A_{i-k}) \cdot \frac{10^6}{T^2} + (B_{i-j} - B_{i-k}) \cdot \frac{10^3}{T} + (C_{i-j} - C_{i-k}) \end{aligned} \quad (6)$$

Minerals involving solid solutions

It has been demonstrated that cation substitution can influence significantly the fractionation between minerals (Friedman & O'Neil, 1977; Zheng, 1993a, 1993b; Kohn & Valley, 1998b, 1998c). Available experimental data for feldspars and muscovite (O'Neil & Taylor, 1967,

1969) and thermodynamic calculations for plagioclase (Ganguly, 1982) show that solid solutions are well approximated by linear interpolation between end-members. Although the effect of cation substitution on $^{18}\text{O}/^{16}\text{O}$ fractionation has been investigated via experiments only for few silicate groups, these relationships are commonly accepted and applied (e.g. Kohn, 1993; Kohn & Valley, 1998b). Hence the isotopic composition of a phase i involving a solid solution with k phase components (end-members) can be recalculated as a linear combination of the oxygen isotope compositions of each end-member $\delta^{18}\text{O}_{k-i}$ (Kohn, 1993)

$$\delta^{18}\text{O}_i = \sum_1^n X_{k-i} \cdot \frac{N_{k-i}}{N_i} \cdot \delta^{18}\text{O}_{k-i} \quad (7)$$

with X_{k-i} the molar fraction of end-member k in phase i , N_{k-i} and N_i the number of moles of oxygen in the end-member k and in phase i . The isotope fractionation parameters between a solid solution i involving k phase components and a pure phase j are obtained from

$$A_{i-j} = \sum_1^k A_{j-i} \cdot X_{k-i} \cdot \frac{N_{k-i}}{N_i} \quad (8)$$

$$B_{i-j} = \sum_1^k B_{j-i} \cdot X_{k-i} \cdot \frac{N_{k-i}}{N_i} \quad (9)$$

$$C_{i-j} = \sum_1^k C_{j-i} \cdot X_{k-i} \cdot \frac{N_{k-i}}{N_i} \quad (10)$$

By combining Equation (4) with Equations (8–10) and assuming the validity of the approximation in Equation (5), the stable isotope fractionation between two phases i (with k phase components) and j (pure) as a function of T becomes:

$$\begin{aligned} \delta^{18}\text{O}_i - \delta^{18}\text{O}_j &\approx \sum_1^k \left(\frac{A_{k-j} \cdot 10^6}{T^2} + \frac{B_{k-j} \cdot 10^3}{T} + C_{k-j} \right) \\ &\quad * X_{k-i} \cdot \frac{N_{k-i}}{N_i} \end{aligned} \quad (11)$$

Equation (11) can be rearranged to obtain a set of linear equations valid for each phase component.

Effect of pressure and salinity in experimental settings

The effect of pressure on oxygen isotope fractionation between minerals has been demonstrated to be small (typically $< 0.2\text{‰}$), particularly at high temperature (Clayton *et al.*, 1975; Polyakov & Kharlashina, 1994; Chacko *et al.*, 2001). Our calculation according to the method of Polyakov & Kharlashina (1994) of pressure-induced deviations between 0.1 and 1.0 GPa at different temperatures for key mineral couples involving quartz confirm this (Table 2). The deviations are higher for quartz/calcite and quartz/rutile than for the silicate/silicate couples, but they are far below typical

uncertainties of the fractionation models, especially at $T \geq 350^\circ\text{C}$. Therefore, the effect of pressure is not considered for the calculation of our database.

Truesdell (1974) investigated the effect of dissolved salts on the oxygen isotope activity ratio of water up to 275°C . The author concluded that most of the salt solutions show a complex behaviour of oxygen isotopes with increasing temperature and that mineral-water fractionations may be affected by shifts up to $\sim 3\text{‰}$ in both the directions. However, this observation is in contrast with other studies investigating different chemical systems. Horita (1989) reviewed 'salt effect' coefficients measured by several authors and investigated the effect of high- CaCl_2 or $-\text{MgCl}_2$ brines on hydrogen and oxygen isotope fractionation factors. The author concluded that NaCl, as well as gypsum, has no effect, although most data were obtained at low temperature (i.e. $< 40^\circ\text{C}$). According to the experiments of Kendall (1983), the presence of NaCl up to 4 molal concentration has no effect on oxygen isotope fractionation between calcite and water at 275°C . Zhang *et al.* (1989) studied experimentally oxygen isotope fractionation between quartz and water, and also concluded that the effect of salinity is not significant at temperature higher than 250°C , whereas it probably affects the rate of oxygen isotope exchange among oxygen-bearing phases. Zhang *et al.* (1994) observed the same effect for the quartz-cassiterite-water and the wolframite-water systems. The experiments performed by Hu & Clayton (2003) show instead that, at elevated temperature and pressure, mineral/mineral fractionation factors derived from separate mineral-'pure' water experiments are not fully compatible because of the different species dissolved in the water in each experiment.

In our database, water is always assumed to be a pure H_2O phase, and experiments performed under different NaCl salinities are still considered. However, because previous studies provide reasons to be cautious about experiments that used brines, such experiments are weighted less than primary data using pure water (see below). Details on the use of brines in experiments are reported in Supplementary Data 1, available for downloading at <http://www.petrology.oxfordjournals.org>.

Table 2: Pressure-induced corrections to the fractionation values at $P = 1\text{ GPa}$ relative to ambient pressure for chosen mineral couples. Calculation by using the method of Polyakov & Khrlashina (1994). Mineral abbreviations from Whitney & Evans (2010)

P-induced corrections at 1 GPa (‰)				
Phase couple	T = 100°C	T = 350°C	T = 600°C	T = 850°C
Qz-Fo	0.05	0.02	0.01	0.00
Qz-Ab	0.06	0.00	0.00	0.00
Qz-En	0.15	0.05	0.03	0.02
Qz-Grs	0.18	0.06	0.03	0.02
Qz-Prp	0.24	0.09	0.05	0.03
Qz-Cal	0.26	0.08	0.04	0.02
Qz-Rt	0.37	0.14	0.07	0.04

TREATMENT OF LITERATURE DATA

Selection of primary data and temperature range

In this study, a wide compilation of published fractionation factors calculated by the methods mentioned above has been produced. Experimental, semi-empirical and natural data (primary data, Fig. 1) have been compiled from the literature for 400 mineral/aqueous fluid and mineral/mineral couples including most major and accessory phases. The complete list of phases is reported in Table 1, the list of all the phase couples in Supplementary Data 1 and 3. All the available fractionation functions between two pure phases or phase end-members were used for the calculation, with the exceptions of calibrations that have been corrected or superseded by later studies, in which case

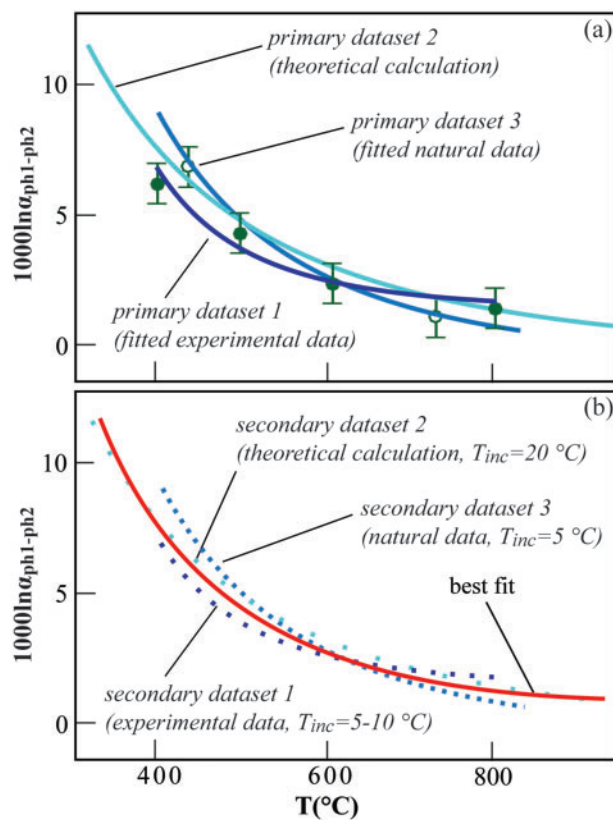


Fig. 1. Generation of secondary data and fitting procedure. (a) All the available oxygen isotope fractionation factors (experimental data, natural studies and semi-empirical calculations) for a phase couple (primary data) have been considered when not inconsistent with the other available data (see text for details). (b) Secondary data points have been generated for each primary dataset by discretizing the fractionation function along the temperature range $[T_{\text{min}}, T_{\text{max}}]$ with a temperature step T_{inc} . This parameter is used as a weighting factor and reflects the degree of confidence of the corresponding primary data. A fixed uncertainty of $\pm 0.3\text{‰}$ was attributed to each secondary data point (not shown in the plot, see text for details). The red line represents the simple interpolation model (second order polynomial fit) to all the secondary data for each phase couple. The results (best fit) of this iterative interpolation are not internally consistent. They represent a first approximation used as input for the global optimization that delivers internal consistency.

only the revised values are reported (i.e. Northrop & Clayton, 1966; O'Neil *et al.*, 1969; Clayton *et al.*, 1972 revised by Friedman & O'Neil, 1977; Zheng, 1999 partially revised by Zheng, 1996; Zheng & Böttcher, 2016 partially revised by Rubatto *et al.*, 2014 and Zheng, 2016) and of calibrations that have been demonstrated to be unreliable (e.g. Shiro & Sakai, 1972; Krylov *et al.*, 2002; Zhou & Zheng, 2003, 2005). Calibrations that have been evaluated but not used for the final calculation are reported in Table 1 in italics and details are given in Supplementary Data 1. Fractionation factors for solid solutions calculated without distinguishing the contribution of each phase component (e.g. Javoy *et al.*, 1970; Bottinga & Javoy, 1975; Kohn & Valley, 1998b) were mostly excluded. In such cases, the fractionation factors are valid only for specific mineral compositions and they can only be used to test the final database.

As discussed above, the fractionation between two phases is generally reported in the literature as a function of T with three parameters A , B and C defined for a temperature range $[T_{min}, T_{max}]$ in which the experiments or the calculation were performed. For the cases where only experimental points were available, A , B and C were calculated by second order polynomial fitting (e.g. Becker and Clayton, 1976; Matthews, 1994). Bond-strength models (e.g. Richter & Hoernes, 1988; Zheng, 1991, 1993a, 1993b, 1999) present equations for calculating fractionation factors between phases over a wide range of temperature (e.g. 0–1200°C), whereas experimental and natural data never exceed the stability region of a phase and are usually even narrower. The temperature range selected for the presented database is between 0°C and 900°C (see discussion below), corresponding to the range where the most experiments have been performed in order to decrease the otherwise overemphasized contribution of the semi-empirical calibrations. None of the primary data from experimental results or natural samples were extrapolated outside the prescribed temperature range, as the parameters are not always valid over a broad temperature range (Clayton, 1981). All the primary data published to be valid outside the chosen temperature range of 0–900°C have been excluded from the calculation or restricted to such range (see Supplementary Data 1 for details).

Theoretically, at infinite T the fractionation between any set of two phases approaches 0‰ and, therefore, many authors questioned the validity of the parameter C in Equation (4) (Sharp, 2017). Whereas the database was optimized assuming $C=0$, no primary data were modified after the published (or revised) functions, because this option was considered as an excessive interference with the primary data.

Generation of secondary data and weighting procedure

The experimental data points used to derive the primary data and their analytical uncertainties are not

systematically available. This prevented the original experimental data points (and their uncertainties) to be used for fitting. Instead, secondary data points were generated for each couple by discretizing the fractionation function along the temperature range $[T_{min}, T_{max}]$ with a temperature step T_{inc} (Fig. 1). Over a given temperature range, the number of secondary $T - \delta^{18}\text{O}$ points increases with decreasing T_{inc} and thus, a function discretized by using a smaller value of T_{inc} will have more weight during the optimization (see below) than a function discretized with a larger value of T_{inc} . This parameter is used as a weighting factor applied to the secondary data reflecting the degree of confidence of the corresponding primary data. If not specified differently in Supplementary Data 1, a T_{inc} value of 5°C was used for well-constrained experimental and natural data, 10°C for synthesis experimental data or experiments with salt added, and 20°C for semi-empirical data.

In addition, a fixed uncertainty of 0.3‰ (2σ) was attributed to each secondary data point, based on the average values proposed in the literature (O'Neil *et al.*, 1969; Savin & Epstein, 1970; Becker & Clayton, 1976; Cole, 1985; Zheng, 1991, 1993b, 1998; Vitali *et al.*, 2000). The uncertainty on the temperature measurement during an experiment is rarely reported in literature and it does not apply to semi-empirical calculations; therefore, uncertainty in T was not taken into account.

Fitting procedure and optimization

Notwithstanding that fractionation factors for mineral couples may be most precise for single, specific mineral compositions, the presence of inconsistency when comparing fractionation factors from different compilations remains an issue. An internally consistent database aims to improve (1) the accuracy by considering numerous independent data and different data types, and (2) the versatility because it can be applied to mineral assemblages without carrying inconsistencies between mineral pairs.

Data processing is required to achieve internal consistency (as defined in the introduction) and it can become prohibitive as large multicomponent systems are involved. Manual evaluations are accordingly confined to small chemical systems or can only be performed infrequently (May and Murray, 2001). In addition, the development of a computational procedure allows the database to be easily updated when new primary data become available.

The internally consistent dataset of fractionation parameters A , B and C (Eq. 4) and their uncertainties were obtained from the secondary data following a three-step procedure: (1) a first iterative approximation of the fractionation parameters; (2) a least-square global optimization; and (3) the calculation of uncertainties by mapping the uncertainty envelopes using a Monte-Carlo (MC) technique. A series of MATLAB®-based

programs were used; short descriptions of each part are given in the following.

Step 1: Iterative approximation of fractionation factors

The first step consists of iteratively applying for each mineral/mineral or mineral/water couple a simple interpolation model to the available secondary data as defined above (Fig. 1). The detailed procedure is illustrated in Fig. SD4-1 in Supplementary Data 4. A reference phase (*REF*) is chosen in order to calculate specific A_{REF-i} and B_{REF-i} ($C_{REF-i}=0$) parameters for each other phase *i*. Quartz was selected as reference phase because (1) it can be considered a pure phase; (2) it is one of the most common rock-forming minerals, with a wide range of *P*–*T* stability; (3) it offers the largest collection of data, derived from different theoretical and experimental methods; and (4) it has been widely used in literature (i.e. proposed fractionation factors for different couples mineral/quartz). It is important to mention that geothermometry or fractionation modelling can be performed in quartz-absent systems using the internally consistent database (after step 2, see below), because every combination of fractionation parameters between all the phases available in the database can be recalculated (see Eq. 6).

Step 2: Global optimization using least squares

Once an approximation of a first solution has been made, a selection criterion or objective function that can be minimized is defined in order to derive a unique and optimal solution (e.g. Berman *et al.*, 1986). The objective function was defined as the sum of the square of the differences between the $\delta^{18}\text{O}$ value Z_i and the modelled $\delta^{18}\text{O}$ value Y_i of the secondary data point *i*.

$$\text{Residual} = \sum_i (Z_i - Y_i)^2 \quad (12)$$

The minimization of this objective function is a non-linear optimization problem, which can be treated with the Nelder–Mead algorithm (Nelder & Mead, 1965). The mineral/mineral or mineral/water couples for which a larger number of secondary data points are available are predominant in constraining the final dataset. The weighing attributed to the different data types (see above) in the generation of secondary data steers the final model to be more heavily determined by experimental and natural data.

Step 3: Determination of minimum uncertainties

Uncertainties on oxygen isotope fractionation parameters serve the important purpose of indicating relative errors, i.e. to know which parameters are better constrained and consistent with available data, and which are less constrained. Unfortunately, most of the studies reporting primary data do not report analytical uncertainties. This lack of constraints prevents the uncertainties to be assessed with the highest rigor. Instead, for

each fractionation couple, a 2σ uncertainty envelope was obtained containing at least 95% of the secondary data points used for fitting.

The regression models are polynomial in one variable (*T*), and their coefficients *A*, *B* and *C* are strongly correlated. Because of this correlation, the coefficients cannot be considered to have independent sources of error. As there exists no standard analytical formula to compute or propagate the uncertainty of polynomial models (see the *Guide to the Expression of Uncertainty in Measurement*, ed. Bureau International des Poids et Mesures, 2008), it can only be estimated via numerical simulation or linearization approximation. To define the 95% uncertainty envelope, a numerical procedure involving MC analysis was used to approximate the uncertainties on each parameter *A*, *B* and *C*. The procedure is illustrated in SD4-2 in Supplementary Data 4.

For each A_{REF-i} , B_{REF-i} and C_{REF-i} , 50 000 random sets of $[\sigma(A_{REF-i}), \sigma(B_{REF-i}), \sigma(C_{REF-i})]$ were generated using a uniform distribution over a range of $\pm 100\%$ (or $\pm 1\%$ when the value was lower than 0.001) for $\sigma(A_{REF-i})$ and $\sigma(B_{REF-i})$ and over the range of $\pm 1\%$ for the parameter $C=0$. This interval for *C* was chosen to contain the average (-0.95%) and the median (0.14%) of the *C* values of all the considered experimental and natural primary data. The uncertainties on the parameters of the couples that do not directly involve the reference mineral (*REF*) were obtained using the following relationships:

$$\sigma(A_{i-j}) = \sqrt{(\sigma(A_{REF-j}) + \sigma(A_{REF-i}))^2} \quad (13)$$

$$\sigma(B_{i-j}) = \sqrt{(\sigma(B_{REF-j}) + \sigma(B_{REF-i}))^2} \quad (14)$$

$$\sigma(C_{i-j}) = \sqrt{(\sigma(C_{REF-j}) + \sigma(C_{REF-i}))^2} \quad (15)$$

Any set of uncertainties $[\sigma(A_{i-j}), \sigma(B_{i-j}), \sigma(C_{i-j})]$ calculated for the phase couple (*i*–*j*) bounds a region with upper and lower limit of $1000 \ln \alpha_{s(u,l)}$ defined as

$$1000 \ln \alpha_{s(u,l)} = \frac{(A_{i-j} \pm \sigma(A_{i-j})) * 10^6}{T^2} + \frac{(B_{i-j} \pm \sigma(B_{i-j})) * 10^3}{T} + (C_{i-j} \pm \sigma(C_{i-j})) \quad (16)$$

The deviation of each secondary data point (coordinates: T_p , $1000 \ln \alpha_p$) from the optimized model ($1000 \ln \alpha_m = f(T)$ in $T = T_p$), noted as DPM (Distance-Point Model), was calculated and compared with the vertical distance (i.e. at fixed *T*) between the envelope $1000 \ln \alpha_s$ and the model $1000 \ln \alpha_m$, noted as DEM (Distance-Envelope Model) (Fig. 2). A randomly generated set of uncertainties $[\sigma(A_{REF-i}), \sigma(B_{REF-i}), \sigma(C_{REF-i})]$ is accepted when $\text{DPM} \leq \text{DEM}$ (i.e. the point lies within the uncertainty envelope) for at least 95% (2σ) of the secondary data points of the couple (*REF*–*i*) and of each other couple involving phase *i*. The fixed uncertainty of 0.3% was considered on each secondary data point

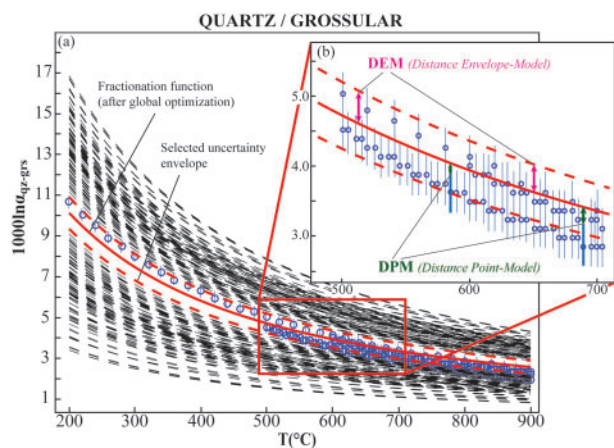


Fig. 2. Determination of *minimum uncertainties*. Quartz/grossular fractionation function is taken as example. (a) Discretized datasets (secondary data) are represented by blue spots. The blue vertical bars represent the fixed uncertainty of $\pm 0.3\text{‰}$ attributed to each secondary data point (see text for details). Our model (optimized fractionation function) is shown as red continuous line. The curves obtained from random generated sets of $[\sigma(A_{REF, i}), \sigma(B_{REF, i}), \sigma(C_{REF, i})]$ are shown as black dashed lines. Only 35 randomly chosen valid uncertainty envelopes (see text for details) are plotted for clarity. The closest one is outlined in red. (b) The Distance-Envelope Model (DEM, pink arrows) represents the vertical distance between our model (red continuous line) and a randomly generated envelope (dotted lines). The Distance-Point Model (DPM, blue arrows) represents the vertical distance between our model and a secondary data point considering the fixed uncertainty on the point of $\pm 0.3\text{‰}$ (green vertical bars). The secondary data points used as reference for showing DEM and DPM are in bold. If $DPM \leq DEM$ for at least 95% of the secondary points, the set of $[\sigma(A_{REF, i}), \sigma(B_{REF, i}), \sigma(C_{REF, i})]$ is accepted. The envelope minimizing the sum of DEMs over the whole temperature range is selected as final set of uncertainties and is marked by the bold dashed lines in (a).

(see above). Among all the accepted sets $[\sigma(A_{REF, i}), \sigma(B_{REF, i}), \sigma(C_{REF, i})]$, the one minimizing DEM over the whole T range was selected as final set of uncertainties (Fig. 2). The absolute values of the uncertainties (at 2σ) are reported in Table 1 and the values of the correspondent residual (Eq. 12) in Supplementary Data 2.

It is important to note that the calculated values of σ represent a minimum absolute uncertainty that is based exclusively on the spread of the available data. The position of each envelope depends on the number and on the spread of the secondary data generated. In cases where fractionation factors are constrained by a single set of secondary data, the calculated uncertainties are expected to be small due to the absence of spread in the data and they might increase when new secondary data are added. Thus, it is important to stress that small uncertainties may be indicative of a lack of constraints rather than of a good agreement among them. Calculated models for couples based on several sets of primary data (see Table 1) are expected to be more accurate, but they might show larger uncertainties due to the distribution of the data. The user of the database is invited to check Table 1 and Supplementary Data 1 and

3 in order to evaluate on how many sets of primary and thus secondary data the reported uncertainties are based.

MODEL RESULTS COMPARED TO PRIMARY DATA

The number of mineral phases and end-members of solid solutions considered in this study (Table 1) is controlled by the availability of oxygen isotope fractionation data. The database (Supplementary Data 2) includes a pure water phase, 25 groups of silicates and 13 single silicate minerals, for a total of 100 pure silicate phases and solid solution end-members, as well as 15 carbonates, 17 oxides, 12 hydroxides, 3 phosphates, 1 salt, and 4 sulphates.

Table 1 presents the model results for the fractionation parameters A and B ($C=0$) (Eq. 4) between quartz and each phase after the optimization for internal consistency, and the calculated minimum absolute uncertainties at the 2σ level (see above). Secondary data and models for key or exemplar phases are shown in Figs 4, 5 and 6. The secondary data and models for all the considered phase couples are reported in Supplementary Data 3.

The calculated fractionation parameters for silicates and carbonates are, in most cases, supported by a diversity of data from different techniques and thus considered to be more robust. Of the major rock-forming minerals, quartz, garnet and pyroxene are based on solid sets of primary data and are inferred to be well constrained. For solid solutions such as amphibole, micas, chlorite, and for minerals of complex chemical composition (e.g. epidote), the primary data are scarce or inconsistent and thus their fractionation factors may lack accuracy or bear a large uncertainty. Mineral groups such as spinel, ilmenite, humite, feldspathoid, pyroxenoid, phenacite, and most of the oxides and hydroxides are uniquely based on semi-empirical datasets by Zheng (1991, 1993a, 1993b, 1996, 1998) because of the lack of experimental and natural data. Experimental or natural data at $T < 200^\circ\text{C}$ are available for fractionations between quartz/water and involving carbonates, chlorite, serpentine, zeolites, few oxides and sulphates. Despite their paucity and possible spread, those data are of key importance beside semi-empirical data for constraining the shape of the fractionation functions, and they improve the quality of the fit also at higher T (see next section).

Further details, addressing in particular the inconsistencies among literature data and the behaviour of the model for those cases are discussed below. Although the parameters for each mineral were derived simultaneously so that every dataset contributed to the refinement of the fractionation properties, the following description is organised by mineral groups. Results are discussed between 200 and 900°C , with emphasis on the stability range for each phase (Figs 3, 4, 5, 6). Results at $T < 200^\circ\text{C}$ are discussed only for quartz/water and calcite/water pairs.

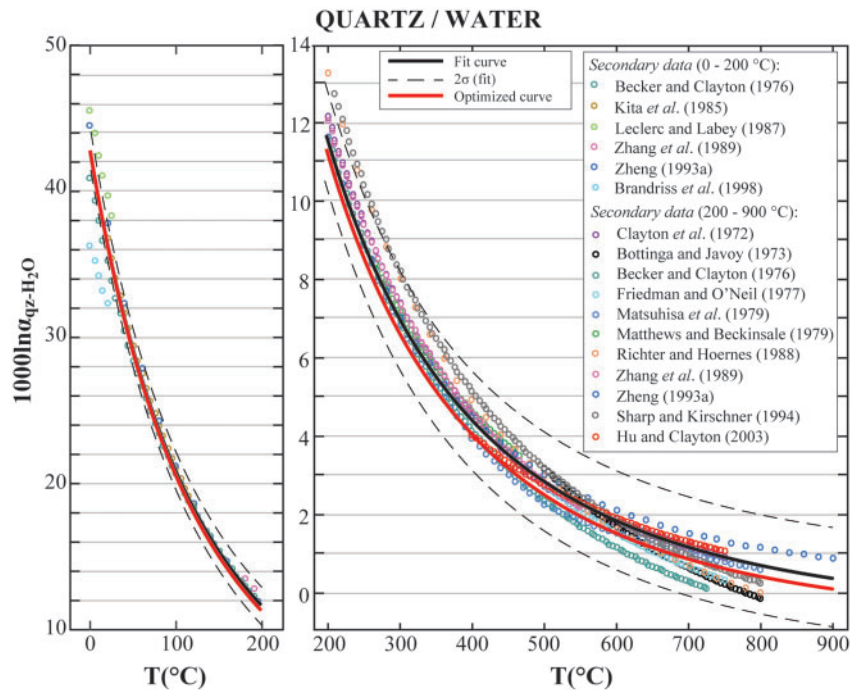


Fig. 3. Quartz/water oxygen isotope fractionation. The fitted function (i.e. only based on quartz/water secondary data, black curve) and the internally consistent model (i.e. obtained by global optimization, red curve) agree within 0.4‰ (see text). The dashed lines represent the 95% prediction interval for the fit.

Anhydrous silicates

Quartz

Quartz was chosen as reference mineral, i.e. the parameters A and B ($C=0$) in Table 1 describe the fractionation between quartz and a phase. The fractionation between quartz and water is the best documented in the literature, with 16 datasets (Table 1) derived with different methods, of which 14 were selected for the optimization. Their good consistency is demonstrated by the low uncertainties on the fit reported in Equation (17) (at 2σ) and plotted in Fig. 3.

The fractionation functions obtained for the couple quartz/water are:

$$1000 \ln \alpha_{qz-H_2O}(fit) = \left(3.98 * \frac{10^6}{T^2} - 2.93 * \frac{10^3}{T} + 0.00 \right) \quad (17)$$

$$1000 \ln \alpha_{qz-H_2O}(opt) = \left(4.11 \pm 0.11 * \frac{10^6}{T^2} - 3.33 \pm 0.61 * \frac{10^3}{T} + 0.00 \pm 0.15 \right) \quad (18)$$

The internally consistent optimized model (*opt*, Eq. 18, uncertainties at 2σ) agrees with the fit of the quartz/water secondary data (*fit*, Eq. 17) within 0.4‰, proving good consistency not only among data for quartz/water, but also among all the data involving quartz (135 couples) and water (147 couples). The uncertainties on the fractionation parameters in Equation (18) incorporate not only the spread of secondary data for this couple, but also for all the other

secondary data involving either quartz or water. Sharp *et al.* (2016) proposed a calibration of the triple oxygen isotope fractionation for quartz/water based on high- T exchange experiments and low- T empirical estimates. All the data considered by the authors are also included in our dataset independently. Our optimized model agrees within 0.5‰ with the calibration proposed by Sharp *et al.* (2016) at $T \geq 200^\circ\text{C}$, and it is 1‰ lower at 60°C .

Theoretically, because mineral polymorphs have a different crystal structure, they are expected to behave differently with respect to oxygen stable isotope fractionation (Shiro & Sakai, 1972; Kawabe, 1978; Smyth, 1989; Zheng, 1993c). Nevertheless, the fractionation functions for α -quartz/water and β -quartz/water proposed by Kawabe (1978) are the same within uncertainty. Other quartz polymorphs are not stable in the T range covered by this database. In addition, no difference in oxygen isotope fractionation between various SiO_2 polymorphs has been measured in natural samples. Thus, only quartz was included in the database and its calibration can be applied to other SiO_2 polymorphs.

Feldspar group

Oxygen isotope fractionation involving albite, anorthite and K-feldspar has been widely investigated with different methods, resulting in a well-documented compilation of fractionation factors (Table 1). Data for feldspar/water oxygen isotope fractionation (O'Neil & Taylor, 1967; Bottinga & Javoy, 1973; Matsuhisa *et al.*, 1979;

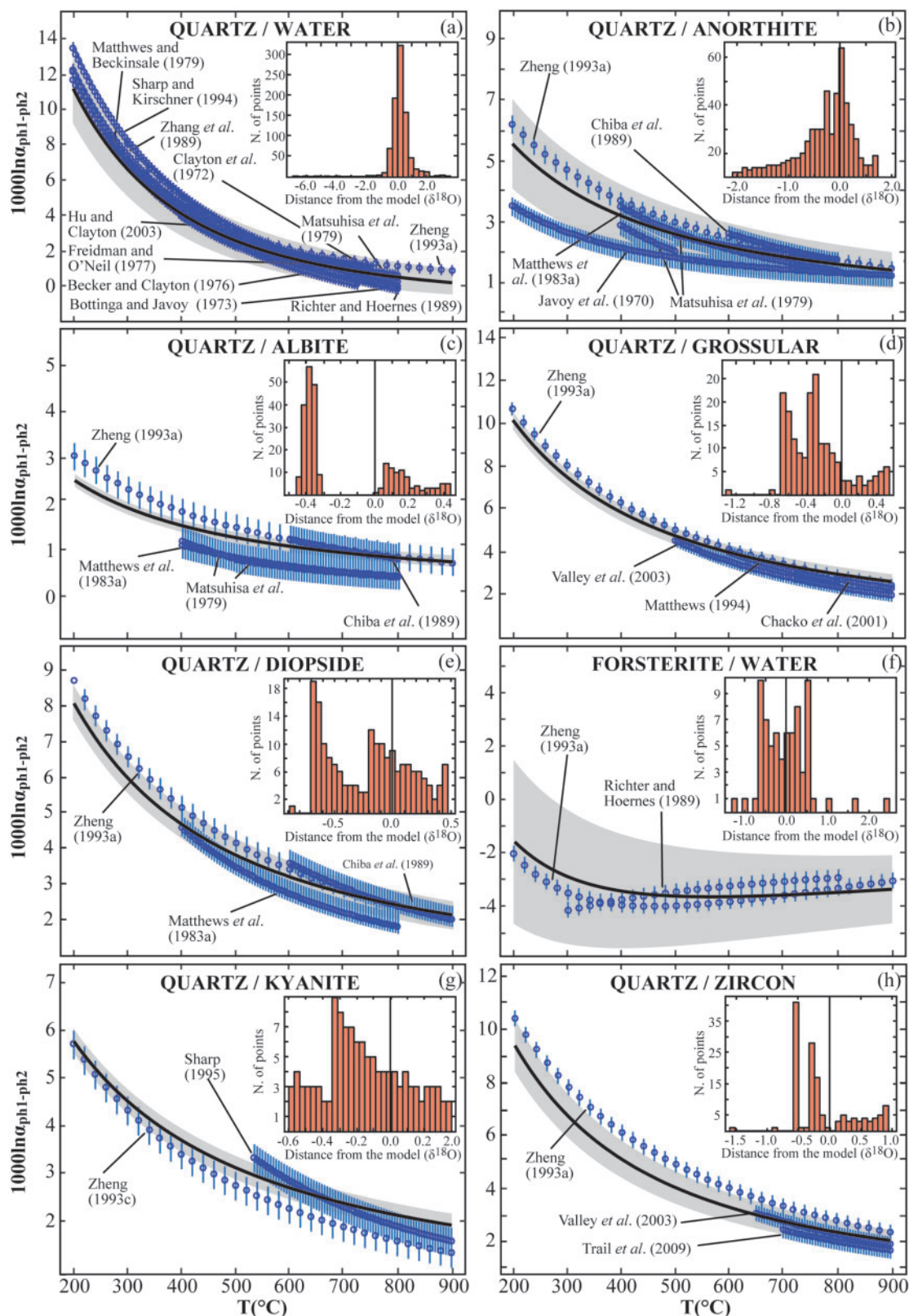


Fig. 4. Secondary data and internally consistent fractionation functions for couples involving selected anhydrous silicates (see text for discussion). Secondary data are reported as blue circles with vertical error bars (assigned fixed uncertainty of $0.3\%_{\text{oor}}$, see text), internally consistent fractionation functions as black lines and uncertainty envelopes (at 2σ) as grey fields. Histograms associated with each plot show the distribution of the secondary data with respect to our model as vertical distance between each point and the model.

Richter & Hoernes, 1988; Zheng, 1993a) are in agreement with each other within 1‰. Data for quartz/feldspar exhibit a scatter caused by small differences in the quartz/water fractionation functions used in each study (Javoy *et al.*, 1970; Matsuhisa *et al.*, 1979; Matthews *et al.*, 1983b; Chiba *et al.*, 1989; Zheng, 1993a) (Supplementary Data 3, page 41). Variations among primary data for the couple quartz/anorthite are up to 2.5‰ at $T=200^{\circ}\text{C}$ and $< 1\text{‰}$ above 600°C (Fig. 4b). The range of primary data for quartz/albite and quartz/K-feldspar is within 0.5‰.

Our fractionation models lie within the range of the secondary data for quartz/anorthite as shown by the histogram in Fig. 4b; the primary data from Javoy *et al.* (1970) are outside the range of uncertainty at $T < 300^{\circ}\text{C}$. Our model for quartz/albite lies in between a bimodal distribution of primary data (Fig. 4c), thus slightly below (0.1–0.3‰) the calibrations of Zheng (1993a) and Chiba *et al.* (1989), but above (0.3–0.6‰) the experimental data of Matsuhisa *et al.* (1979) and Matthews *et al.* (1983b) (Fig. 4c). The fractionation calculated for quartz/K-feldspar is within the range of the primary data at $T > 400^{\circ}\text{C}$ and up to 0.4‰ lower at lower T .

Garnet group

Beside semi-empirical data, natural and few experimental calibrations for garnet end-members are also available (Lichtenstein & Hoernes, 1992; Matthews, 1994; Rosenbaum & Matthey, 1995; Chacko *et al.*, 2001; Valley *et al.*, 2003), but both approaches are limited for the purpose of this study as only data for garnet close to the composition of a pure end-member were used for fitting. The considered semi-empirical and experimental data agree with each other within 1‰, with the exception of spessartine/water, for which the data disagree by 1.5‰ (Fig. 4d).

The calculated models fit within the range of the primary data above 500°C for each couple involving grossular, almandine, pyrope, spessartine, andradite, uvarovite and melanite end-members (Fig. 4d, Supplementary Data 3, pages 43–61).

Pyroxene group

Primary experimental and semi-empirical data for clinopyroxene are in good agreement (Fig. 4e), with a maximum mismatch of $\sim 1\text{‰}$ between primary data for quartz/jadeite (see Supplementary Data 3, page 156). Our models for clinopyroxene are centred with respect to the primary data for the clinopyroxene/water and quartz/cclinopyroxene couples; secondary data from Matthews *et al.* (1983a) systematically lie below the model and are partially outside the uncertainty range (see Fig. 4e).

Few data are available for fractionation involving the orthopyroxene end-members enstatite and ferrosilite (Richter & Hoernes, 1988; Zheng, 1993a) (Table 1). The divergence between primary data at low T is not significant since orthopyroxene is not stable at $T < 500^{\circ}\text{C}$. At

$T > 500^{\circ}\text{C}$, our models are centred with respect to the data and the secondary data points are within 0.5‰.

Olivine group

Semi-empirical calculations by Richter & Hoernes (1988) and Zheng (1993a) describing the fractionation between fayalite/water and forsterite/water agree within 0.5‰ between 400 and 800°C despite having an opposite concavity (Fig. 4f). Those describing the fractionation between quartz/forsterite and quartz/fayalite agree within 1‰ at $T > 500^{\circ}\text{C}$. Experimental data for fractionation between quartz/forsterite and calcite/forsterite (Chiba *et al.*, 1989; Zhang *et al.*, 1994) are in line with semi-empirical calculations for this temperature range. Our models diverge from Richter & Hoernes (1988) and Zheng (1993a) toward fractionations approaching 0‰ with increasing T . Our fractionation models involving tephroite are reproducing the secondary data within 0.5‰ at $T > 500^{\circ}\text{C}$.

Al₂SiO₅-polymorphs

Mostly semi-empirical data are available for Al₂SiO₅-polymorphs (Richter & Hoernes, 1988; Zheng, 1993c; Hoffbauer *et al.*, 1994), with a notable paucity of experimental and natural constraints (Sharp, 1995; Tennie *et al.*, 1998). Semi-empirical calculation of Richter & Hoernes (1988) for fractionation between andalusite/water, kyanite/water and sillimanite/water are in good agreement with the model of Zheng (1993c) (Fig. 4g, Supplementary Data 3, pages 177–185). The spread of primary data increases up to 2‰ for the quartz/mineral functions of Sharp (1995) and Zheng (1993c) and up to 1.5‰ for the calcite/mineral functions of Hoffbauer *et al.* (1994) and Zheng (1993c). Experimental data for calcite/kyanite by Tennie *et al.* (1998) are in agreement with semi-empirical data by Hoffbauer *et al.* (1994). According to the fractionation factors calculated using incremental methods (Richter & Hoernes, 1988; Zheng, 1993c; Hoffbauer *et al.*, 1994) fractionation is expected between the different Al₂SiO₅ polymorphs (i.e. 1‰ at 500°C between kyanite and sillimanite). However, such differences have not been observed in nature (Sharp, 1995; Cavosie *et al.*, 2002).

Our models for Al₂SiO₅/water are close to the functions of Zheng (1993c) and Richter & Hoernes (1988). Secondary data from Hoffbauer *et al.* (1994) and Tennie *et al.* (1998) for calcite/Al₂SiO₅ lie systematically above our models (1–1.5‰) and part of them are out the uncertainty window. Our models for quartz/Al₂SiO₅ approach the data of Sharp (1995) and diverge from Zheng (1993c) up to 0.8‰ with increasing T (Fig. 4g, Supplementary Data 3, pages 177–185). The calculated fractionation between andalusite/kyanite and andalusite/sillimanite are $< 0.8\text{‰}$ at $T > 200^{\circ}\text{C}$.

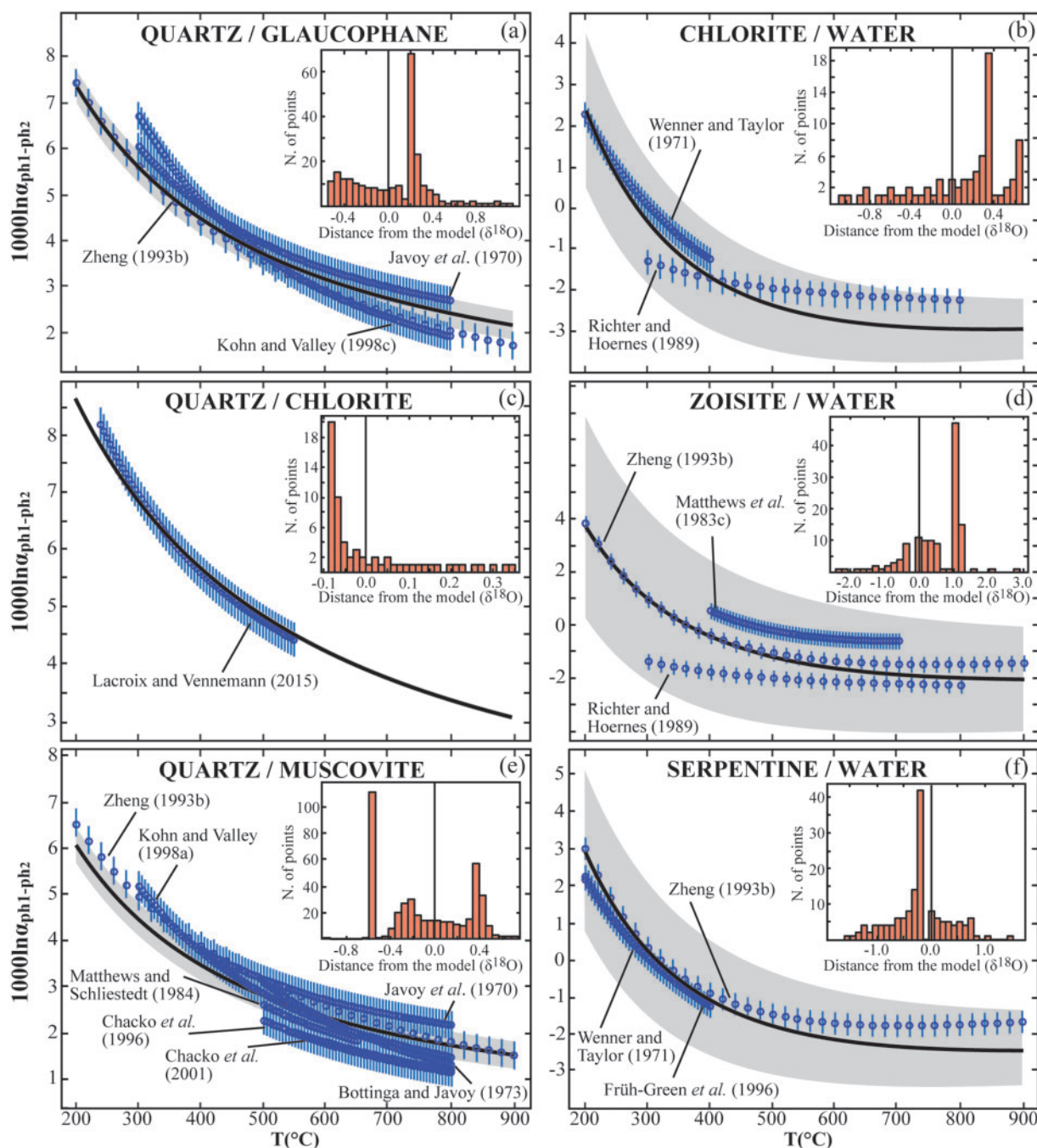


Fig. 5. Secondary data and internally consistent fractionation functions for couples involving hydrous silicates (see text for discussion). Secondary data are reported as blue circles with vertical error bars (assigned fixed uncertainty of 0.3‰, see text), internally consistent fractionation functions as black lines and uncertainty envelopes (at 2σ) as grey fields. Histograms associated with each plot show the distribution of the secondary data with respect to our model as vertical distance between each point and the model.

Zircon

For fractionation between quartz/zircon, natural data by Valley et al. (2003) agree within 0.6‰ with the model of Zheng (1993a). The experimental study of Trail et al. (2009) is lower than the natural calibration of Valley et al. (2003) by ~ 0.5 ‰ (Fig. 4h). Semi-empirical data (Richter & Hoernes, 1988; Zheng, 1993a) are available for zircon/water fractionation (Table 1). The model of

Zheng (1993a) predicts lower fractionation with a shift up to 4‰ at 400°C and of ~ 2 ‰ at 600°C (see Supplementary Data 3, page 374).

Our model for quartz/zircon predicts a lower fractionation than Zheng (1993a), close to the data of Valley et al. (2003) (Fig. 4h). The model for zircon/water lies between the calibrations of Zheng (1993a) and Richter & Hoernes (1988).

Hydroxyl-bearing silicates

Amphibole group

Available fractionation data involving amphibole are mostly limited to the semi-empirical calculations proposed by Richter & Hoernes (1988), Zheng (1993b) and Hoffbauer *et al.* (1994). Natural data are only available for glaucophane (Kohn & Valley, 1998a), and the agreement with the semi-empirical data is within 1‰ (Fig. 5a).

Our models are largely consistent with all these data, with a maximum difference of $\sim 0.5\text{‰}$. The fractionation predicted by our model for quartz/glaucophane is within the range defined by semi-empirical and natural data. The model is closer to the fractionation functions of Zheng (1993b) and Javoy *et al.* (1970), up to 1‰ lower than Kohn & Valley (1998c) at $T < 500^\circ\text{C}$, and follows the calibration of Javoy *et al.* (1970) above 500°C (Fig. 5a).

Chlorite group

Oxygen isotope fractionation factors involving chlorite group minerals have been calculated by Zheng (1993b). Natural data are available for chlorite/water (Wenner & Taylor, 1971) and quartz/chlorite fractionation (Lacroix & Vennemann, 2015), without distinction between chlorite end-members. The chlorite end-members listed above and a generic chlorite have been included in the dataset. Data for chlorite/water from Wenner & Taylor (1971) predict a significantly higher fractionation than the calculation of Richter & Hoernes (1988), up to 3‰ at $T < 300^\circ\text{C}$ (Fig. 5b).

Our models for quartz/chlorite end-members differ from the secondary data by less than 0.5‰ . For chlorite/water, our model follows the calibration of Wenner & Taylor (1971) at $T < 400^\circ\text{C}$, and it is up to 0.5‰ smaller than the calibration of Richter & Hoernes (1988) at higher $T > 200^\circ\text{C}$ (Fig. 5b). Fractionation predicted by our model for quartz/chlorite agrees within 0.2‰ with the natural data of Lacroix & Vennemann (2015) (Fig. 5c).

Epidote group

Semi-empirical, experimental and natural data are available for oxygen isotope fractionation involving epidote and zoisite. The experimental calibrations by Matthews *et al.* (1983c) for mineral/water fractionation is up to 2‰ higher than the calibration of Zheng (1993b) between 500 and 800°C , but the model of Richter & Hoernes (1988) is significantly lower than the other available data below 500°C (Fig. 5d). The calibration of Zheng (1993b) for calcite/zoisite agrees with the one of Matthews (1994) within 0.3‰ , while it is $\sim 2.5\text{‰}$ higher for quartz/zoisite. Our model for zoisite/water is within the primary data range (Fig. 5d), and the one for quartz/zoisite is close to the data of Matthews (1994) (Supplementary Data 3, page 68). The scatter of the secondary data causes large uncertainties on the fractionation parameters (Table 1).

Mica group

The different types of primary data are mostly within 1.5‰ of each other for each mica type (e.g. Fig. 5e). Notable exceptions are the fractionation functions involving margarite, with differences up to 3‰ (Richter & Hoernes, 1988; Zheng, 1993b; Hoffbauer *et al.*, 1994), and paragonite/water (O'Neil & Taylor, 1969; Richter & Hoernes, 1988; Zheng, 1993b), with a mismatch up to 2‰ at 350°C , which decreases with increasing T .

Our model predicts intermediate fractionation values for the mica/water couples. Calculated fractionation functions for calcite/mica couples are systematically lower ($0.5\text{--}1\text{‰}$) than the data of Hoffbauer *et al.* (1994). Our model for quartz/muscovite lies in the middle of the available primary data between 500 and 800°C (Fig. 5e).

Serpentine group

A limited amount of semi-empirical (Richter & Hoernes, 1988; Zheng, 1993b) and natural data (Wenner & Taylor, 1971; Früh-Green *et al.*, 1996), and no experimental data for oxygen isotope fractionation are available for serpentine (Table 1). Zheng (1993b) calculated fractionation factors for amesite, lizardite and serpentine (of antigorite structure) versus water, quartz and calcite. Data for amesite/water fractionation from Zheng (1993b) are consistent within 1‰ with those from Richter & Hoernes (1988) at $T > 400^\circ\text{C}$. Natural data for serpentine/water fractionation by Wenner & Taylor (1971) and Früh-Green *et al.* (1996) agree within 1‰ with the calculation of Zheng (1993b) (Fig. 5f). The only dataset involving chrysotile is from Richter & Hoernes (1988) for chrysotile/water.

More than one set of primary data is available for the serpentine/water and amesite/water couples, and our models lies close to the calibration of Zheng (1993b) up to 400°C , and diverge toward lower values at higher T (Fig. 5f). Our model for chrysotile/water shows an opposite concavity with respect to the primary data of Richter & Hoernes (1988), but the fit is within 0.3‰ in the range of the secondary data (see Supplementary Data 3, page 338).

Carbonates

Calcite and dolomite

Calcite is the second most documented mineral for oxygen isotope fractionation experiments and calculations after quartz and the first among carbonates, followed by dolomite (Table 1). Data for calcite/water fractionation (Fig. 6a) show a good consistency and are mostly derived from experimental data (Epstein *et al.*, 1953; Northrop & Clayton, 1966; O'Neil *et al.*, 1969; Kim & O'Neil, 1997; Hu & Clayton, 2003). Conversely, the secondary data for quartz/calcite fractionation are more scattered (Fig. 6b), especially at low T (up to 2‰). This is caused by (1) the use of independent experimental data for quartz/water and calcite/water fractionation, (2) large uncertainties on T for natural samples (e.g. Sharp & Kirschner, 1994), or

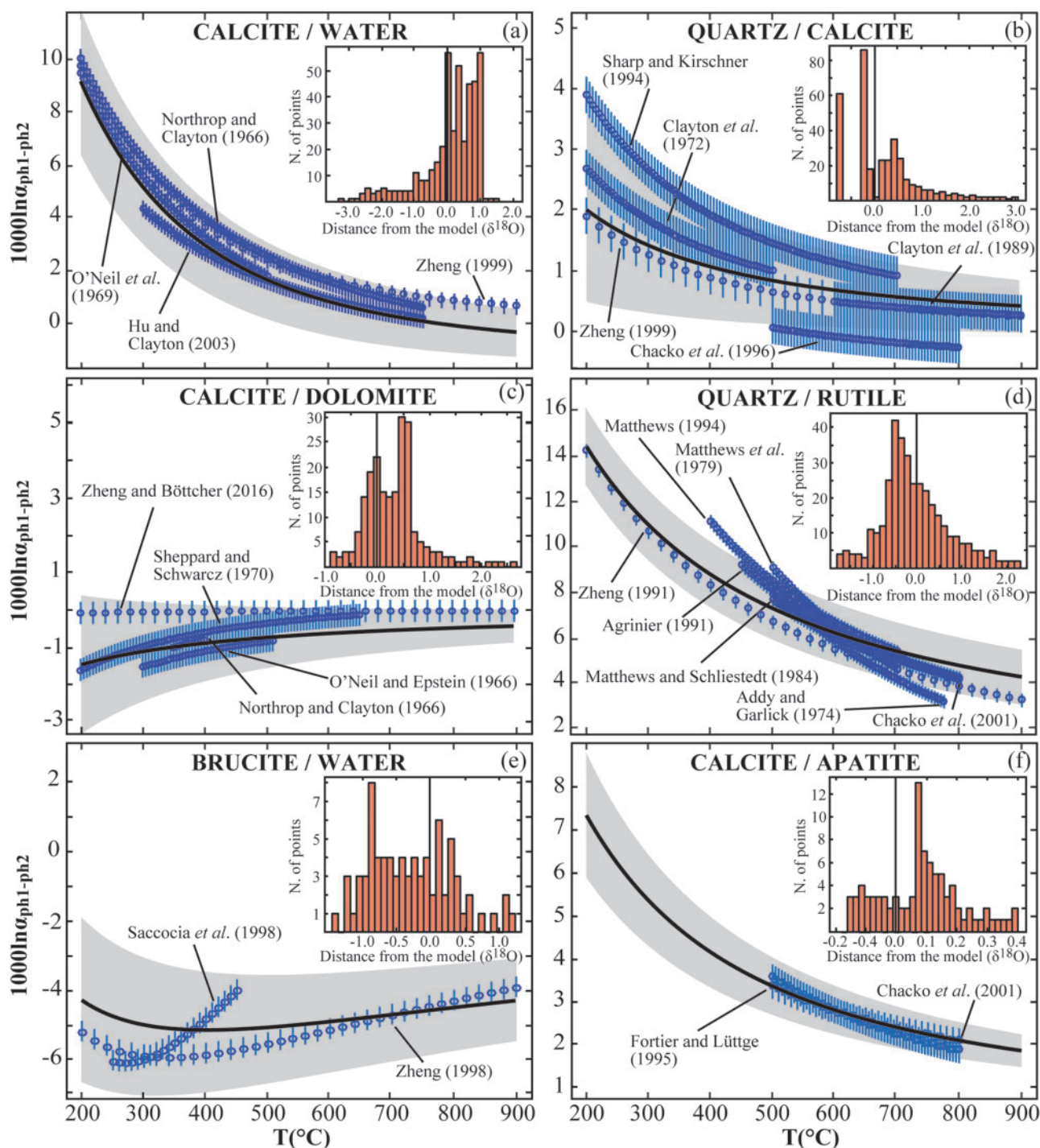


Fig. 6. Secondary data and internally consistent fractionation functions for couples involving selected non-silicate minerals (see text for discussion). Secondary data are reported as blue circles with vertical error bars (assigned fixed uncertainty of 0.3‰ , see text), internally consistent fractionation functions as black lines and uncertainty envelopes (at 2σ) as grey fields. Histograms associated with each plot show the distribution of the secondary data with respect to our model as vertical distance between each point and the model.

(3) incomplete isotopic equilibration in experiments and natural samples (e.g. Northrop & Clayton, 1966; Kim & O'Neil, 1997; Hu & Clayton, 2003). The fractionation between calcite and dolomite derived from experimental and natural data (Northrop & Clayton, 1966; O'Neil & Epstein, 1966; Sheppard & Schwarcz,

1970) is up to 3‰ lower (at 100°C) than the one calculated by Zheng & Böttcher (2016) (Fig. 6c).

Our model for calcite/water is close to the calibration of Hu & Clayton (2003) at $T > 450^\circ\text{C}$, causing a systematic shift of -1‰ with respect to the data of Northrop & Clayton (1966) and Zheng (1999). Between 200 and

400°C, our model approaches the calibration of O'Neil *et al.* (1969) (Fig. 6a). Regarding calcite/water fractionation at low T (10–40°C), Coplen (2007) suggested that previous experimental and many biological empirical equations may suffer from a kinetic effect, underestimating the fractionation value of $\sim 2\text{‰}$. Our model in this temperature range fits the calibration of Coplen (2007) (see Supplementary Data 3, page 3), pointing to its consistency with the other data involving calcite or water. Our model for quartz/calcite has to accommodate the scattering primary data and ends up close to the fractionation function of Zheng (1999) and Clayton *et al.* (1989). The secondary data of Sharp & Kirschner (1994) are above our model and partially outside the uncertainty range. By contrast, the model of Chacko *et al.* (1996) is significantly lower (1‰) and outside the uncertainty range (Fig. 6b). Our model for calcite/dolomite is within the range of the experimental data up to 350°C, and up to 0.8‰ lower at higher T (Fig. 6c). This discrepancy can be related to the abundant data available for dolomite/water fractionation that contribute to define the fractionation functions.

Oxides

Iron oxides

Most of the primary data for oxygen isotope fractionation between magnetite and quartz, water or calcite agree within 2‰ in the range of 500 to 900°C. Only the empirical calibration of Bottinga & Javoy (1973) for magnetite/water fractionation is discordant and has been excluded from the optimization. Data for quartz/magnetite diverge at lower T , up to 8‰ between the calibrations of Zheng (1991) and Chiba *et al.* (1989). Our model for quartz/magnetite is centred with respect to the secondary data at $T > 500^\circ\text{C}$ and fits the calibration of Zheng (1991) at lower T (see Supplementary Data 3, page 295). Our model for calcite/magnetite is up to 0.5‰ higher than the highest batch of secondary data (Zheng, 1991), and for magnetite/water the mismatch with the data is within 1‰. These deviations are caused by the abundance of data for quartz/magnetite that controls the other fractionation functions involving magnetite.

The hematite/water fractionation function at $T < 200^\circ\text{C}$ predicted by Zheng (1991) is dramatically lower (up to 14‰) than experimental data by Yapp (1990) and Bao & Koch (1999) and the studies on natural samples by Clayton & Epstein (1961) with a scattered distribution (see Supplementary Data 3, page 283). Our model plots close to the experimental secondary data at low T , but with a large associated uncertainty derived from the scattering of the data. This large uncertainty represents a serious limitation for the modelling and use of $\delta^{18}\text{O}$ of hematite in geochemical studies.

Titanium oxides

Data for oxygen isotope fractionation involving rutile show a poor agreement between the semi-empirical

calculations of Zheng (1991) and the more consistent sets of experimental and natural data (Addy & Garlick, 1974; Matthews *et al.*, 1979; Matthews & Schliestedt, 1984; Agrinier, 1991; Bird *et al.*, 1994; Matthews, 1994; Chacko *et al.*, 2001) (i.e. quartz/rutile, Fig. 6d). In particular, semi-empirical rutile/water fractionation data (Zheng, 1991) show an opposite trend with respect to the experimental data (Addy & Garlick, 1974; Matthews *et al.*, 1979), which are instead consistent with each other (see Supplementary Data 3, page 307). Considering the consistency between the calculations of Zheng (1991) and Bird *et al.* (1994) at low T and between the data of Addy & Garlick (1974) and Matthews *et al.* (1979) in the 450–800°C range, no primary data was excluded from the optimization.

Our models are centred with respect to the secondary data for each couple involving rutile (see histogram in Fig. 6d for quartz/rutile). The resulting curve for rutile/water follows the function of Zheng (1991) within 0.5‰, proving a better agreement of this dataset with the primary data available for quartz/rutile (Addy & Garlick, 1974; Matthews *et al.*, 1979; Matthews & Schliestedt, 1984; Agrinier, 1991; Zheng, 1991; Matthews, 1994; Chacko *et al.*, 2001) (Fig. 6d) and for calcite/rutile (Zheng, 1991; Matthews, 1994; Chacko *et al.*, 2001) (see Supplementary Data 3, page 308).

Hydroxides

Most of the data for hydroxide minerals are from Zheng (1998) (Table 1). New experimental and/or natural data are required for improving the quality of the present data.

Brucite

Four sets of primary data are available for brucite/water fractionation (Savin & Lee, 1988; Saccocia *et al.*, 1998; Zheng, 1998; Xu & Zheng, 1999). The results of the two semi-empirical methods from Savin & Lee (1988) and Zheng (1998) are a remarkably different in slope and absolute values (up to $\sim 5\text{‰}$ at 200°C and $\sim 4\text{‰}$ at 450°C). A detailed discussion on the equation proposed by Savin & Lee (1988) is available in Zheng (1998). The calculation of Zheng (1998) was preferred because of better agreement with experimental data (Saccocia *et al.*, 1998; Xu & Zheng, 1999). The dataset of Savin & Lee (1988) was, therefore, excluded for the optimization. Our model for brucite/water agrees within 1‰ with the data from Zheng (1998) and Xu & Zheng (1999) at $T < 150^\circ\text{C}$, while it predicts higher fractionation values (up to 1‰) than Zheng (1998) up to 600°C due to the influence of the experimental data by Saccocia *et al.* (1998) (Fig. 6e).

Phosphates

Apatite

The only experimental data available for apatite are from Fortier & Lüttge (1995). Chacko *et al.* (2001) proposed an equation obtained by linear interpolation of

those experimental points. Fractionation factors involving F-apatite, Cl-apatite and OH-apatite were calculated by Zheng (1996). These different types of apatite have not been implemented in the database and the model relies on experimental data. Our model for calcite/apatite is up to 0.5‰ higher than the secondary data, and the one for quartz/apatite up to 0.3‰ higher (Fig. 6f, Supplementary Data 3, page 216).

Monazite

Fractionation factors for monazite are based on the datasets by Breecker & Sharp (2007) and Rubatto *et al.* (2014). In the latter, the authors propose a revision to the previous calculation by Zheng (1996), which was, therefore, not considered in our calculation. Our model agrees within 0.5‰ with the calibration of Breecker & Sharp (2007) at $T > 500^\circ\text{C}$, being $\sim 0.8\text{‰}$ higher than the data of Rubatto *et al.* (2014) (Supplementary Data 3, page 218).

PRECISION AND ACCURACY OF THE APPLICATIONS

Temperature range

As mentioned above, experimental or natural data at $T < 200^\circ\text{C}$ are available for few phases and typically exhibit a larger spread with respect to data obtained at higher T . Despite those limitations, low- T data are of key importance beside semi-empirical calculations for constraining the shape of the calculated fractionation functions, which should flatten out at increasing T because the fractionation between two phases decreases. During the global optimization, the best fit among all the data is achieved with no additional constraints on the convexity or concavity of the functions other than the secondary data. When the fractionation between two phases is small at $T > 200^\circ\text{C}$, i.e. the function curvature is less pronounced, the solution that minimizes the sum of the overall residuals without considering the low- T data may result in a function with opposite curvature with respect to the primary data. Therefore, considering low- T data overall improves the match between the shape of the primary data and our model. Nevertheless, we do not recommend applying the database at $T < 200^\circ\text{C}$. Furthermore, in this T range oxygen isotope fractionation between phases can be larger than 10‰ and the relation in Equation (5) is no longer robust. The validity of the approximation in Equation (5) and the reliability of the fit, together with the cause of possibly large uncertainties, must be evaluated by examining the results reported in Supplementary Data 3.

The choice of a maximum temperature of 900°C limits the contribution of the carbonate-exchange experiments by Clayton *et al.* (1989) performed at temperature up to 1000°C , those of Chiba *et al.* (1989), Gautason *et al.* (1993), Rosenbaum & Mathey (1995), Chacko *et al.* (2001) and Breecker & Sharp (2007)

performed up to 1200°C , and the piston-cylinder experiments of Breecker & Sharp (2007) (quartz/monazite fractionation) and Trail *et al.* (2009) (quartz/zircon fractionation) performed up to 1000°C . The importance of these primary data is still recognized and they are all included and discretized up to 900°C . However, they represent less than 10 % of the experimental data. Extending the T range would overemphasize the contribution of the semi-empirical calibrations at high T .

Thermometry

The temperature of equilibration between two phases i and j can be retrieved by inverting Equation (4), provided that their oxygen isotopic compositions are known. Assuming the validity of the approximation in Equation (5), T can be calculated as

$$T = 10^{3*} \left(\frac{-B_{i-j} \pm \sqrt{B_{i-j}^2 - 4A_{i-j}*(C_{i-j} - (\delta^{18}\text{O}_i - \delta^{18}\text{O}_j))}}{2A_{i-j}} \right)^{-1} \quad (19)$$

The inversion results in two solutions for T , of which only one is meaningful for geological interpretation (i.e. real and positive number).

A MATLAB®-based Graphical User Interface (GUI) software THERMOX (Fig. SD4-3 in Supplementary Data 4) is distributed together with the internally consistent database. The equilibrium temperature and related uncertainties can be obtained from oxygen isotope data of two minerals among all the available ones in the database. Because the calculation performed by THERMOX and based on our database (1) considers solid solutions, (2) determines uncertainties, (3) allows the use of phase couples for which no direct experimental or natural data are available, and (4) calculates the uncertainty also on the fractionation functions for such phase couples, it offers some advantages over existing databases compiling fractionation functions for individual mineral pairs.

The equilibrium temperature is calculated from Equation (19) and reported with three uncertainties: (1) *absolute uncertainty*, (2) *relative uncertainty*, and (3) *total uncertainty* (Fig. 7, Fig. SD4-3 in Supplementary Data 4). The *absolute uncertainty* reflects the precision of the fractionation function compared to the primary data and is determined from the uncertainties on the parameters A , B and C (Table 1). The *relative uncertainty* reflects the quality of the isotopic analyses and is based on the analytical uncertainties on the measured $\delta^{18}\text{O}$ values. The combination of the *absolute* and *relative* uncertainties results in a *total uncertainty* on the calculated equilibrium temperature. Because the fractionation function is not linear, the calculated upper and lower uncertainties in temperature (*UAU* and *LAU* for *absolute uncertainty*; *URU* and *LRU* for *relative uncertainty*; *UTU* and *LTU* for *total uncertainty*) are not symmetric.

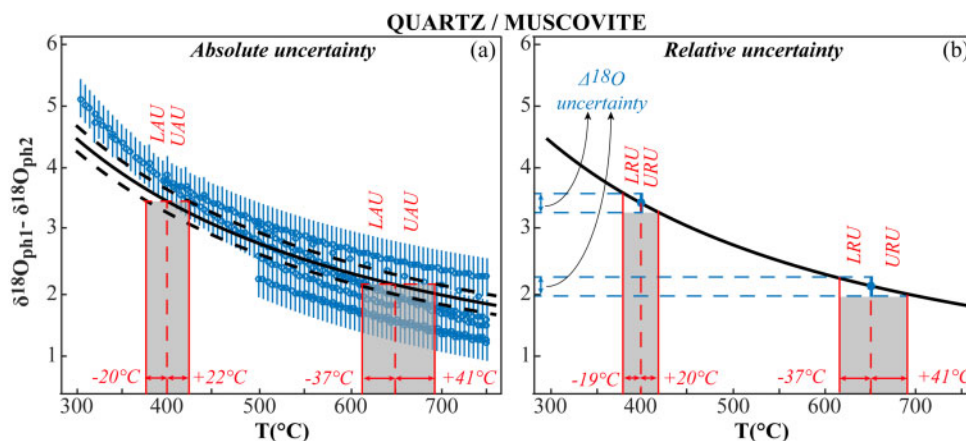


Fig. 7. Uncertainty on equilibrium temperature calculated by THERMOX. The mineral couple quartz/muscovite is taken as example. The approximation reported in Equation (5) is valid for this couple. (a) The *absolute uncertainty* depends on the uncertainty envelope (represented at 1σ , black dotted lines) and on the slope of the function (black continuous line). The Upper Absolute Uncertainty (UAU) and Lower Absolute Uncertainty (LAU) (at 1σ) are shown for $T = 400^\circ\text{C}$ and 650°C . Blue dots represent secondary data with the assigned fixed uncertainty (see text for details). (b) The *relative uncertainty* depends on the $\delta^{18}\text{O}$ measurement uncertainties for the two considered minerals and on the slope of the function. The oxygen isotope fractionation uncertainty (blue marks) is the uncertainty on the difference $\delta^{18}\text{O}_{\text{ph1}} - \delta^{18}\text{O}_{\text{ph2}}$ calculated as the square root of the quadratic sum of the uncertainties on $\Delta^{18}\text{O} = \delta^{18}\text{O}_{\text{ph1}}$ and $\delta^{18}\text{O}_{\text{ph2}}$. The Upper Relative Uncertainty (URU) and Lower Relative Uncertainty (LRU) (at 1σ) are shown for $T = 400^\circ\text{C}$ and 650°C .

A number of factors directly influence accuracy and precision of the results. The assumption of $C=0$ forces our model to diverge from primary data for which $C \neq 0$ (largely represented by semi-empirical data). This in turn causes an increase of the uncertainty on A and B . Additionally, the global optimization method has an effect on the different mineral/mineral fractionation factors. The multi-dimensional fit produces a database consistent with the secondary data, but it may also lead to shifts in fractionation values and larger uncertainties for specific mineral couples than otherwise obtained by fitting a single set of experiments or natural data.

The precision of oxygen isotope thermometry is related to the mathematical expression of the oxygen isotope fractionation functions, which are quadratic functions with a variation in slope (i.e. the value of the derivative) at changing T depending on the coefficients A and B . Fractionation functions having a steeper slope ($\Delta'_{i,j}$) are less sensitive to minor changes in $\Delta^{18}\text{O}_{i,j}$, generating more precise temperature results. The effects of the slope on precision are illustrated in Fig. 8. The shift in the temperature calculated that results from a variation of 0.2‰ in $\Delta^{18}\text{O}_{i,j}$ at 600°C was quantified for different couples with decreasing slopes assuming the relation in Equation (5) valid. As already discussed, the fractionation function (Eq. 4) has a horizontal asymptote $C = 0$ for $T \rightarrow \infty$, so that its shape is flatter at higher T , and, therefore, the same variation in $\Delta^{18}\text{O}_{i,j}$ produces larger shifts at higher T (Fig. 7). This decrease in precision affects the uncertainty of the temperature estimates for high- T mineral assemblages.

If solid solutions are involved, the molar fractions of each end-member are used to recalculate the fractionation of the mineral (see Eq. 11). The application of the fractionation model to solid solutions requires the

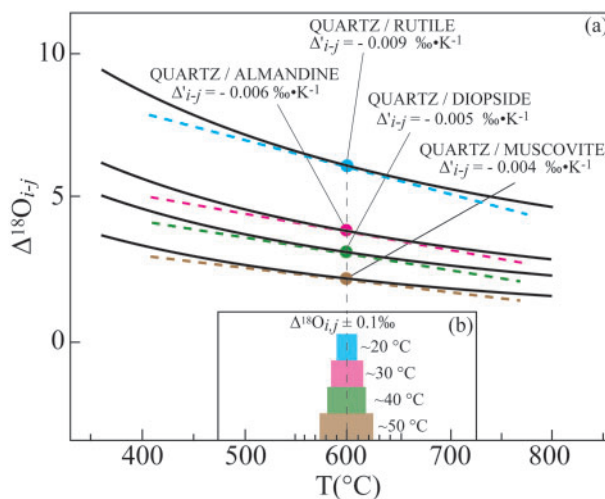


Fig. 8. Dependence of the precision of isotopic thermometry on the slope of the fractionation function. (a) Oxygen isotope fractionation functions (black curves) for quartz/muscovite, quartz/diopsid, quartz/almandine and quartz/rutile and their derivative $\Delta'_{i,j}$ (coloured dashed lines) at $T = 600^\circ\text{C}$ (assuming the validity of the approximation in Eq. 5). Higher values of $\Delta'_{i,j}$ correspond to steeper slopes. (b) Sensitivity of isotopic thermometry to a variation in $\Delta^{18}\text{O}_{i,j}$ of 0.2‰ at $T = 600^\circ\text{C}$ for each couple shown in (a). The sensitivity decreases with increasing value of $\Delta'_{i,j}$.

propagation of the uncertainties on the fractionation of single end-members. Aside from this, the accuracy of the results may depend on the choice of end-member fractions. Considering the same $\Delta^{18}\text{O}_{i,j}$ between quartz and different garnet end-members, the calculated equilibrium temperatures vary by a maximum of 30°C between 450 and 550°C for andradite, almandine, grossular, spessartine and uvarovite. This variation is in the same order of magnitude of the absolute

uncertainties of the models for each garnet end-member at the same T (20 to 30°C). Exceptions are the quartz/pyrope and quartz/melanite pairs, for which the calculated temperatures are 30 to 50°C higher and lower, respectively than the average temperature obtained by using the other end-members. Thus, for the specific case of garnet, the chosen end-member proportions have a limited effect on the result. Other mineral groups show a different behaviour. Assuming equal $\Delta^{18}O_{i-j}$ between quartz/muscovite (assumed as pure K-white mica end-member), quartz/paragonite (assumed as pure Na-white mica end-member) and quartz/phengite (assumed as K-Mg-white mica), the calculated equilibrium T in the same temperature range for quartz/muscovite differs by $\sim 40^\circ\text{C}$ and $\sim 50^\circ\text{C}$ from the result for quartz/paragonite and quartz/phengite. These differences are larger than the uncertainties of each model ($\sim 30^\circ\text{C}$) and the correct composition of white mica needs to be used. Such effects are even larger for the clinopyroxene group. Calculated equilibrium temperatures for quartz/acmite and quartz/jadeite are consistent with each other within uncertainty, but $\sim 300^\circ\text{C}$ lower than those calculated using quartz/diopside or quartz/hedenbergite for the same difference in isotopic composition of each of these pairs. Significant differences are noted for plagioclase and amphiboles. In such cases, the use of solid solutions instead of pure end-members alone is of key importance to produce meaningful results.

Application of oxygen isotope fractionation factors to natural samples

The oxygen isotopic composition of a mineral in sedimentary, magmatic and metamorphic systems is controlled by several factors (e.g. Savin & Epstein, 1970): (1) the bulk isotopic composition of the reactive part of the rock (excluding detrital/inherited unreactive material, i.e. mineral relics or cores of growing porphyroblasts) and the coexisting minerals; (2) the isotopic composition of the fluid; and (3) the formation temperature or the temperature at which isotopic exchange by diffusion stopped. Therefore, the interpretation of measured values in natural samples based on modelling results that rely on our (or any other) database for oxygen isotope fractionation requires detailed petrography and petrology, including textural observation, investigation of major and trace element compositions, comparison of results from thermodynamic modelling with the observed assemblages and compositions. In-situ analysis of $\delta^{18}\text{O}$ at the sub-mineral scale, most commonly by ion microprobe, is a fundamental tool for oxygen isotope studies of natural samples where minerals exhibit complex textures, preserve intergranular zoning and mineral relics (e.g. Baumgartner & Valley, 2001; Russell *et al.*, 2013; Rubatto & Angiboust, 2015; Quinn *et al.*, 2017).

As the oxygen isotope fractionation between phases changes with T as well as the stable mineral assemblage, compositional and isotopic zoning is expected in

minerals that grew over a wide T range (e.g. Kohn, 1993; Vho *et al.*, 2020). The original isotopic zoning may be later affected by oxygen diffusion. However, constraints on diffusivity of ^{18}O are few and limited to some minerals (e.g. Farver & Giletti, 1985; Farver, 1989; Fortier & Giletti, 1991; Vielzeuf *et al.*, 2005). Measured isotopic profiles within single mineral grains may help us to understand to which extent diffusion changed the original $^{18}\text{O}/^{16}\text{O}$ composition (e.g. Valley & Graham, 1993; Peck *et al.*, 2003; Vielzeuf *et al.*, 2005; Desbois *et al.*, 2007; Russell *et al.*, 2013; Higashino *et al.*, 2019). Additionally, post-growth chemical re-equilibration of major cations does not necessarily imply oxygen isotope equilibrium.

All these factors make assessing the assumption of isotopic equilibrium in complex metamorphic rocks a challenging task. The present database can be an efficient tool to explore which mineral couples are in apparent isotopic equilibrium from the measured oxygen isotope composition of different minerals or mineral zones.

The accuracy of the fractionation functions generated by our model is directly linked to the quality of both the constraints (primary data) and our procedure for data processing. Published data reporting oxygen isotope compositions of various mineral couples from localities of known P - T conditions of equilibration can be used to test the accuracy of the fractionation factors derived from our model. Equilibrium temperatures were re-evaluated for the Yakou in Rizhao eclogite (Sulu terrane, eastern China) by combining various $\delta^{18}\text{O}$ mineral compositions published by Zheng *et al.* (2002). The calculated temperatures using our database are $425 \pm 20^\circ\text{C}$ for quartz/muscovite, $430 \pm 35^\circ\text{C}$ for quartz/omphacite and $460 \pm 20^\circ\text{C}$ for quartz/garnet (both for core and rim composition, Enami *et al.*, 1993). The results for garnet/muscovite and garnet/omphacite are consistent but associated to a large uncertainty ($> 100^\circ\text{C}$) due to the limited fractionation between those mineral pairs. Temperatures obtained by different mineral couples are consistent with each other and point to a re-equilibration stage during the retrograde path as already proposed for this area (Enami *et al.*, 1993 and references therein). A similar test was run for three samples of eclogite from Trescolmen (Adula Nappe, Swiss Alps) using the isotopic compositions of Kohn & Valley (1998b). Average temperatures of $560 \pm 50^\circ\text{C}$ and $560 \pm 40^\circ\text{C}$ were obtained by oxygen isotope fractionation modelling of omphacite/quartz and quartz/rutile, respectively. The results are in line with the peak metamorphic conditions of 550–650°C reported for this area (Heinrich, 1986). It is important, however, to notice that garnet and zoisite in the Trescolmen eclogite show major element zoning (Zack *et al.*, 2002) and their $\delta^{18}\text{O}$ values cannot necessarily be linked to a single growth stage (see above).

To conclude, despite previous considerations regarding the possibility of dealing with large uncertainties, the internally consistent database largely matches previous calculations based on selected mineral/mineral

oxygen isotope fractionation or equilibrium T obtained from independent constraints.

Limitations and alternative strategies

Calculation of an extensive, comprehensive and internally-consistent dataset is not straightforward and unavoidably relies on decisions on primary data validity and processing procedures. This section addresses potential limitations and discusses possible directions to be explored in future studies.

The problem of reliability of semi-empirical data has been discussed in the literature. Chacko *et al.* (1996, 2001) showed that the increment method is most robust for anhydrous silicates, but may give inaccurate results for hydrous silicates, oxides and phosphates. Chacko & Deines (2008) argued that the increment method's predictions are also poor for carbonates. To minimize this shortfall, we adopted two strategies: (1) a relative heavier weight is given to experimental data vs. natural and semi-empirical data; and (2) the T range of our calibration has been limited to an interval that is compatible with most experimental studies, avoiding the calibration curve to be overwhelmed by semi-empirical data (see section 'Temperature range'). The final result is that mismatches between semi-empirical and other primary data are mostly within 1‰ also for hydrous silicates and exceptions are reported in the model results section. Incremental calculations are less reliable for oxides, and experimental and natural data are available only for a few oxides. For apatite and monazite, the available natural and experimental calibrations are integrated in our model beside semi-empirical data. However, oxides and phosphates generally occur in low modal abundance in natural rocks and thus, the uncertainty associated with their oxygen fractionation has a very minor weight when modelling multi-phase systems (see below).

A novelty in our approach is the implementation of uncertainties on isotope fractionation factors and the clarification of their statistical meaning. The results show that for the most constrained phases, a precision of 0.5–1.0‰ (2σ) is achieved. This level of precision may appear large for petrological applications, but is actually comparable to the final uncertainties associated with in-situ measurements by ion microprobe (i.e. obtained by adding internal and external uncertainties), which are rarely better than 0.5‰ (2σ), especially for minerals affected by matrix-related mass fractionation such as garnet (e.g. Page *et al.*, 2010; Martin *et al.*, 2014). Larger uncertainties due to discrepancies between available data must be carefully evaluated when the model is applied. Discrepancies between the model and the data that occur outside the stability field of single phases are irrelevant, as pointed out above for major minerals, such as pyroxene, feldspar and garnet.

Implementation of the presented approach and testing of alternative strategies could be considered in the

future for improving the precision and the accuracy of the calculated fractionation factors.

In this study, Equation (4) was chosen as it is the most commonly used expression for describing oxygen isotope fractionation and fitting most of the experimental data (see above). It has been proposed that mineral-pair fractionation at $T > 300\text{--}400^\circ\text{C}$ is better described by a linear relation in the space $1/T^2$ (e.g. Chacko *et al.*, 2001). However, mineral/water fractionation is not linear in the $1/T^2$ space, and a linear dependence in the space $1/T$ better represents mineral-pair fractionation at low T (e.g. Chacko *et al.*, 2001). Equation (4) with $C=0$ represents the best expression for fitting our dataset, which includes mineral/water fractionation data and covers a large temperature range. Further work could investigate the possibility of using two different linear equations, one in the space $1/T^2$ at high T and one in the space $1/T$ for low T . This would imply choosing a T threshold valid for all the considered phases, excluding mineral/water fractionation data and might require a re-assessment of published experimental data not fitted following these equations.

Further constraints could be added to the calculation, for instance, based on chemical-isotopic exchanges (e.g. Kohn & Valley, 1998a, 1998b, 1998c). The fractionation behaviour of some phases can be determined through combined chemical and isotopic exchanges based on the known fractionation factors of other phases. This method could, for example, provide 'constraints' to end-members for which no good experimental or semi-empirical data are available. On the other hand, this approach raises the problem of treating primary data not fully consistent with chemical-isotopic exchanges and quantifying the potential bias introduced by selecting the 'well known' phases. It has to be mentioned that deviations from chemical-isotopic exchange constraints in our model are generally within the given uncertainties.

A different approach to reduce the reliance on semi-empirical calibrations would be to use semi-empirical data only in the temperature ranges covered by experimental or empirical data, assigning them suitable uncertainties and then regressing data using weighted regressions. This would likely require a linear fit in the space $1/T^2$ and an intercept fixed at 0, instead of Equation (4) chosen for this calculation, as a large set of sparse data points may not provide enough constraints for a correct estimate of two parameters (i.e. A and B). Additional attempts could be made by also considering data for mineral pairs beside quartz/mineral and calcite/mineral, although they are a minority. Those data mostly come from natural samples with their associated geological uncertainty.

PERSPECTIVE: COUPLING THERMODYNAMIC AND OXYGEN FORWARD MODELLING

The database for oxygen isotope fractionation between minerals that we present can be applied in a

Table 3: Predicted stable mineral assemblage, mineral compositions and mineral proportions for an average pelite (Ague, 1991) with a $\delta^{18}\text{O}$ bulk value of 12‰. Mineral composition of solid solutions is reported only when used in the oxygen modelling calculation. $\delta^{18}\text{O}$ values are reported in ‰ relative to VSMOW. STAGE 1: $P=0.9\text{ GPa}$, $T=800^\circ\text{C}$; STAGE 2: $P=2.0\text{ GPa}$, $T=550^\circ\text{C}$. Abbreviations from Whitney & Evans (2010)

	Stable assemblage	Mineral composition	Vol%	Mol%	$\delta^{18}\text{O}$ (‰)
STAGE 1	Quartz	–	20.0	50.9	13.8
	Sanidine	$\text{Ab}_{26}\text{An}_2\text{Sa}_{72}$	26.4	14.7	12.8
	Plagioclase	$\text{Ab}_{64}\text{An}_{30}\text{Sa}_6$	17.6	10.3	12.7
	Garnet	$\text{Grs}_6\text{Prp}_{29}\text{Alm}_{63}\text{Sps}_2$	17.5	8.9	10.7
	Biotite	–	10.6	4.2	10.5
	Sillimanite	–	7.4	8.8	12.1
	Rutile	–	0.8	2.3	9.1
	Quartz	–	21.1	61.5	14.3
STAGE 2	Garnet	$\text{Grs}_{18}\text{Prp}_{14}\text{Alm}_{66}\text{Sps}_2$	17.6	9.8	9.9
	Phengite	–	39.2	18.6	11.5
	Paragonite	–	8.3	4.2	11.5
	Glaucofane	–	13.0	3.2	10.9
	Rutile	–	0.8	2.7	7.7

thermodynamic framework to model the evolution of $\delta^{18}\text{O}$ in minerals. Thermodynamic modelling can be combined with $\delta^{18}\text{O}$ modelling to calculate changes in $\delta^{18}\text{O}$ of minerals in addition to their composition and modal abundance in metamorphic systems (Kohn, 1993; Vho *et al.*, 2020). At fixed P , T and bulk-rock composition, the mineral assemblage, mineral modes and compositions can be determined using Gibbs free energy minimization (e.g. de Capitani & Brown, 1987). Knowledge of the mineral modes, mineral composition and T evolution allow the isotope partitioning among the phases of the system to be calculated using Equation (11) at every step of the rock evolution. The conservation of the $\delta^{18}\text{O}$ in the system can be described as

$$\delta^{18}O_{\text{sys}} * N_{\text{sys}} = \sum_{k=1}^p M_k * N_k * \delta^{18}O_k \quad (20)$$

where $\delta^{18}O_{\text{sys}}$ is the isotopic composition of the system ($\delta^{18}\text{O}$ bulk), N_{sys} the total number of moles of oxygen in the system, p is the number of phases, M_k the number of moles of phase k , N_k the its number of oxygen and $\delta^{18}O_k$ its oxygen isotope composition (Kohn, 1993). When the differential of Equation (20) is equal to 0, the system is maintained closed with respect to oxygen isotopes. Open-system behaviour can be modelled either by setting the differential of Equation (20) equal to a non-zero value (open with respect to oxygen isotopes) or by changing the number of moles of the phases in the rock (open with respect to the chemical composition of the system). For instance, open-system models can describe the effect of fluid released (or introduced) during metamorphic processes or fractional crystallization. Given a specific bulk-rock $\delta^{18}\text{O}$, the $\delta^{18}\text{O}$ values of each phase of the stable assemblage can be calculated by solving the linear system containing 1 Equation of type (20) and $P-1$ Equations of type (11). If solid solutions are involved, the system will predict the oxygen isotope composition of each end-member. If the $\delta^{18}\text{O}$ of one phase is known, it is possible to model the $\delta^{18}\text{O}$ of the

other phases in equilibrium and the bulk $\delta^{18}\text{O}$ by solving the same linear system (Vho *et al.*, 2020).

An example is given in Table 3. A bulk $\delta^{18}\text{O}$ of 12.0‰ was attributed to an ‘average pelite’ (composition from Ague, 1991). The stable mineral assemblage, composition and modal abundances of minerals and their $\delta^{18}\text{O}$ values have been modelled at granulite-facies conditions (stage 1, 0.9 GPa and 800°C) and subsequently at eclogite-facies conditions (stage 2, 2.0 GPa and 550°C). A closed system with respect to both oxygen isotope and chemical composition has been assumed. Thermodynamic modelling was performed by using Theriak-Domino (de Capitani & Brown, 1987; de Capitani & Petrakakis, 2010) and the internally consistent dataset of Holland & Powell (1998) (tc55, distributed with Theriak-Domino 04.02.2017). No mineral fractionation was considered, i.e. the whole volume of rock was assumed to fully re-equilibrate at any change in P – T conditions. The oxygen isotope composition of each mineral phase was calculated using the fractionation factors reported in Table 1. The change in the $\delta^{18}\text{O}$ value of each mineral between the two stages depends on changes in T and mineral assemblage. Assuming a closed system, the largest changes between stage 1 and stage 2 are predicted for rutile ($\sim 1.4\text{‰}$). The $\delta^{18}\text{O}$ value of garnet is modified by only $\sim 0.8\text{‰}$ from stage 1 to stage 2. This demonstrates that change in T alone can only produce a limited shift (i.e. $\leq 1.0\text{‰}$) in the oxygen isotope composition of garnet, in agreement with published estimates (e.g. Kohn, 1993; Russell *et al.*, 2013). Further processes (e.g. mineral and fluid fractionation, input of external fluid of different isotopic composition) are needed to produce larger variations. The predicted $\delta^{18}\text{O}$ values of cogenetic phases for a given bulk $\delta^{18}\text{O}$ can be compared with data from mineral and mineral-zone analyses in natural samples. Deviations from the models may identify open-system processes, which can then be further investigated with additional isotope and petrologic techniques (Kohn, 1993). These results provide a theoretical basis for evaluating to what extent a rock has evolved either as an open

system with respect to oxygen isotopes or as a closed system fully or partially re-equilibrated.

CONCLUSIONS

Advanced applications of oxygen isotope fractionation to natural samples, such as combined thermodynamic and oxygen isotope modelling, requires consideration of the entire mineral assemblages rather than individual mineral pairs. We demonstrate that it is possible to refine the oxygen isotope fractionation factors between several minerals in a consistent way. A considerable effort was made for critical assessment of all the relevant primary data and for their transformation into an internally consistent database including 153 mineral phases and a pure water fluid phase. The main steps needed to produce the presented database are:

1. The selection of primary data (fractionation factors) from published semi-empirical, experimental and natural studies of oxygen isotope fractionation between mineral/mineral and mineral/water couples;
2. The generation of secondary data points by discretizing the fractionation function for each phase couple along the temperature range [T_{min} , T_{max}] and using a different density of temperature steps T_{inc} as a weighting factor;
3. The fitting of the secondary data and the global optimization by least-square to achieve internal consistency;
4. The calculation of uncertainties by using a Monte-Carlo technique.

Comparisons with published data on oxygen isotope compositions of minerals in select natural samples indicate that the fractionation factors calculated with this approach are robust in that they successfully match natural observations. In order to facilitate calculations, the program THERMOX was developed to compute equilibrium temperature modelling, also considering solid solutions, and to calculate the related uncertainties.

The obtained database can be applied to model the evolution of $\delta^{18}\text{O}$ in minerals through their metamorphic history in the recommended T range of 200–900°C, and provides a theoretical base for evaluating to what extent a rock has evolved either as an open system with respect to oxygen isotopes or as a closed system fully or partially re-equilibrated.

ACKNOWLEDGEMENTS

We thank J. Hermann for helpful conversations and Reto Giere for careful editorial handling. We are grateful to Ulrich Linden for his technical support. J.W. Valley, Z. Sharp, Y.F. Zheng, A. Matthews, M. Kohn, T. Chacko and four anonymous reviewers are warmly thanked for their insightful reviews that helped to improve the database and the manuscript.

FUNDING

This work was supported by the Swiss National Science Foundation [Project N. 200021_166280].

SUPPLEMENTARY DATA

Supplementary data are available at *Journal of Petrology* online.

REFERENCES

- Addy, S. K. & Garlick, G. D. (1974). Oxygen isotope fractionation between rutile and water. *Contributions to Mineralogy and Petrology* **45**, 119–121.
- Agrinier, P. (1991). The natural calibration of $^{18}\text{O}/^{16}\text{O}$ geothermometers: application to the quartz-rutile mineral pair. *Chemical Geology* **91**, 49–64.
- Ague, J. J. (1991). Evidence for major mass transfer and volume strain during regional metamorphism of pelites. *Geology* **19**, 855–858.
- Bao, H. & Koch, P. L. (1999). Oxygen isotope fractionation in ferric oxide-water systems: low temperature synthesis. *Geochimica et Cosmochimica Acta* **63**, 599–613.
- Baumgartner, L. P. & Valley, J. W. (2001). Stable isotope transport and contact metamorphic fluid flow. *Reviews in Mineralogy and Geochemistry* **43**, 415–467.
- Becker, R. H. & Clayton, R. N. (1976). Oxygen isotope study of a Precambrian banded iron-formation, Hamersley Range, Western Australia. *Geochimica et Cosmochimica Acta* **40**, 1153–1165.
- Berman, R. G. (1988). Internally-Consistent Thermodynamic Data for Minerals in the System $\text{Na}_2\text{O}-\text{K}_2\text{O}-\text{CaO}-\text{MgO}-\text{FeO}-\text{Fe}_2\text{O}_3-\text{Al}_2\text{O}_3-\text{SiO}_2-\text{TiO}_2-\text{H}_2\text{O}-\text{CO}_2$. *Journal of Petrology* **29**, 445–522. [10.1093/petrology/29.2.445](https://doi.org/10.1093/petrology/29.2.445)
- Berman, R. G., Engi, M., Greenwood, H. J. & Brown, T. H. (1986). Derivation of internally-consistent thermodynamic data by the technique of mathematical programming: a review with application the system $\text{MgO}-\text{SiO}_2-\text{H}_2\text{O}$. *Journal of Petrology* **27**, 1331–1364.
- Bigeleisen, J. & Mayer, M. G. (1947). Calculation of equilibrium constants for isotopic exchange reactions. *The Journal of Chemical Physics* **15**, 261–267.
- Bird, M. I., Longstaffe, F. J. & Fyfe, W. S. (1993). Oxygen-isotope fractionation in titanium-oxide minerals at low temperature. *Geochimica et Cosmochimica Acta* **57**, 3083–3091.
- Bird, M. I., Longstaffe, F. J., Fyfe, W. S., Tazaki, K. & Chivas, A. R. (1994). Oxygen-isotope fractionation in gibbsite: synthesis experiments versus natural samples. *Geochimica et Cosmochimica Acta* **58**, 5267–5277.
- Bötcher, M. E. (2000). Stable isotope fractionation during experimental formation of Norsethite ($\text{BaMg}[\text{CO}_3]_2$): a mineral analogue of dolomite. *Aquatic Geochemistry* **6**, 201–212.
- Bottinga, Y. & Javoy, M. (1973). Comments on oxygen isotope geothermometry. *Earth and Planetary Science Letters* **20**, 250–265.
- Bottinga, Y. & Javoy, M. (1975). Oxygen isotope partitioning among the minerals in igneous and metamorphic rocks. *Reviews of Geophysics* **13**, 401–418.
- Brandriss, M. E., O'Neil, J. R., Edlund, M. B. & Stoermer, E. F. (1998). Oxygen isotope fractionation between diatomaceous silica and water. *Geochimica et Cosmochimica Acta* **62**, 1119–1125.
- Breecker, D. O. & Sharp, Z. D. (2007). A monazite oxygen isotope thermometer. *American Mineralogist* **92**, 1561–1572.

- Carothers, W. W., Adami, L. H. & Rosenbauer, R. J. (1988). Experimental oxygen isotope fractionation between siderite-water and phosphoric acid liberated CO₂-siderite. *Geochimica et Cosmochimica Acta* **52**, 2445–2450.
- Cavosie, A. J., Sharp, Z. D. & Selverstone, J. (2002). Co-existing aluminum silicates in quartz veins: a quantitative approach for determining andalusite-sillimanite equilibrium in natural samples using oxygen isotopes. *American Mineralogist* **87**, 417–423.
- Chacko, T., Cole, D. R. & Horita, J. (2001). Equilibrium oxygen, hydrogen and carbon isotope fractionation factors applicable to geologic systems. *Reviews in Mineralogy and Geochemistry* **43**, 1–81.
- Chacko, T. & Deines, P. (2008). Theoretical calculation of oxygen isotope fractionation factors in carbonate systems. *Geochimica et Cosmochimica Acta* **72**, 3642–3660.
- Chacko, T., Hu, X., Mayeda, T. K., Clayton, R. N. & Goldsmith, J. R. (1996). Oxygen isotope fractionations in muscovite, phlogopite, and rutile. *Geochimica et Cosmochimica Acta* **60**, 2595–2608.
- Chiba, H., Chacko, T., Clayton, R. N. & Goldsmith, J. R. (1989). Oxygen isotope fractionations involving diopside, forsterite, magnetite, and calcite: application to geothermometry. *Geochimica et Cosmochimica Acta* **53**, 2985–2995.
- Chiba, H., Kusakabe, M., Hirano, S.-I., Matsuo, S. & Somiya, S. (1981). Oxygen isotope fractionation factors between anhydrite and water from 100 to 550°C. *Earth and Planetary Science Letters* **53**, 55–62.
- Clayton, R. N. (1961). Oxygen isotope fractionation between calcium carbonate and water. *The Journal of Chemical Physics* **34**, 724–726.
- Clayton, R. N. (1981). *Isotopic Thermometry. Thermodynamics of Minerals and Melts*. New York, NY: Springer, 85–109.
- Clayton, R. N. & Epstein, S. (1961). The use of oxygen isotopes in high-temperature geological thermometry. *The Journal of Geology* **69**, 447–452.
- Clayton, R. N., Goldsmith, J. R., Karel, K. J., Mayeda, T. K. & Robert C, N. (1975). Limits on the effect of pressure on isotopic fractionation. *Geochimica et Cosmochimica Acta* **39**, 1197–1201.
- Clayton, R. N., Goldsmith, J. R. & Mayeda, T. K. (1989). Oxygen isotope fractionation in quartz, albite, anorthite and calcite. *Geochimica et Cosmochimica Acta* **53**, 725–733.
- Clayton, R. N. & Kieffer, S. W. (1991). Oxygen isotopic thermometer calibrations. *Stable Isotope Geochemistry: A Tribute to Samuel Epstein* **3**, 1–10.
- Clayton, R. N., O'Neil, J. R. & Mayeda, T. K. (1972). Oxygen isotope exchange between quartz and water. *Journal of Geophysical Research* **77**, 3057–3067.
- Cole, D. R. (1985). Preliminary evaluation of oxygen isotopic exchange between chlorite and water. *Geological Society of America, Abstracts with Programs (United States)* **17**, No. CONF-8510489.
- Cole, D. R., Mottl, M. J. & Ohmoto, H. (1987). Isotopic exchange in mineral-fluid systems. II. Oxygen and hydrogen isotopic investigation of the experimental basalt-seawater system. *Geochimica et Cosmochimica Acta* **51**, 1523–1538.
- Coplen, T. B. (2007). Calibration of the calcite–water oxygen-isotope geothermometer at Devils Hole, Nevada, a natural laboratory. *Geochimica et Cosmochimica Acta* **71**, 3948–3957.
- Criss, R. E. (1999). *Principles of Stable Isotope Distribution*. Oxford: Oxford University Press on Demand.
- de Capitani, C. & Brown, T. H. (1987). The computation of chemical equilibrium in complex systems containing non-ideal solutions. *Geochimica et Cosmochimica Acta* **51**, 2639–2652.
- de Capitani, C. & Petrakakis, K. (2010). The computation of equilibrium assemblage diagrams with Theriak/Domino software. *American Mineralogist* **95**, 1006–1016.
- Desbois, G., Ingrin, J., Kita, N. T., Valley, J. W. & Delouie, E. (2007). New constraints on metamorphic history of Adirondack diopsides (New York, U.S.A.): Al and δ¹⁸O profiles. *American Mineralogist* **92**, 453–459.
- Eiler, J. M., Baumgartner, L. P. & Valley, J. W. (1992). Intercrystalline stable isotope diffusion: a fast grain boundary model. *Contributions to Mineralogy and Petrology* **112**, 543–557.
- Eiler, J. M., Valley, J. W. & Baumgartner, L. P. (1993). A new look at stable isotope thermometry. *Geochimica et Cosmochimica Acta* **57**, 2571–2583.
- Enami, M., Zang, Q. & Yin, Y. (1993). High-pressure eclogites in northern Jiangsu–southern Shandong province, eastern China. *Journal of Metamorphic Geology* **11**, 589–603.
- Engl, M. (1992). Thermodynamic Data for Minerals: A Critical Assessment. *The Stability of Minerals*. Dordrecht: Springer, 267–328.
- Epstein, S., Buchsbaum, R., Lowenstam, H. A. & Urey, H. C. (1953). Revised carbonate-water isotopic temperature scale. *Geological Society of America Bulletin* **64**, 1315–1326.
- Escande, M., Decarreau, A. & Labeyrie, L. (1984). Etude Experimentale de L'échangeabilité des Isotopes de L'oxygene des Smectites. *Comptes-rendus des séances de l'Académie des sciences. Série 2. Mécanique-Physique, Chimie, Sciences de L'univers, Sciences de la Terre* **299**, 707–710.
- Eslinger, E. V. (1971). Mineralogy and oxygen isotope ratios of hydrothermal and low-grade metamorphic argillaceous rocks. Ph.D. thesis, Case Western Reserve University, Cleveland.
- Eslinger, E. V. & Savin, S. M. (1973). Mineralogy and oxygen isotope geochemistry of the hydrothermally altered rocks of the Ohaki-Broadlands, New Zealand, geothermal area. *American Journal of Science* **273**, 240–267.
- Farver, J. R. (1989). Oxygen self-diffusion in diopside with application to cooling rate determinations. *Earth and Planetary Science Letters* **92**, 386–396.
- Farver, J. R. & Giletti, B. J. (1985). Oxygen diffusion in amphiboles. *Geochimica et Cosmochimica Acta* **49**, 1403–1411.
- Fayek, M. & Kyser, T. K. (2000). Low temperature oxygen isotopic fractionation in the uraninite–UO₃–CO₂–H₂O system. *Geochimica et Cosmochimica Acta* **64**, 2185–2197.
- Feng, X. & Savin, S. M. (1993). Oxygen isotope studies of zeolites—Stilbite, analcime, heulandite, and clinoptilolite: III. Oxygen isotope fractionation between stilbite and water or water vapor. *Geochimica et Cosmochimica Acta* **57**, 4239–4247.
- Fortier, S. M. & Giletti, B. J. (1991). Volume self-diffusion of oxygen in biotite, muscovite, and phlogopite micas. *Geochimica et Cosmochimica Acta* **55**, 1319–1330.
- Fortier, S. M. & Lüttge, A. (1995). An experimental calibration of the temperature dependence of oxygen isotope fractionation between apatite and calcite at high temperatures (350–800°C). *Chemical Geology* **125**, 281–290.
- Fortier, S. M., Lüttge, A., Satir, M. & Metz, P. (1994). Oxygen isotope fractionation between fluorphlogopite and calcite: an experimental investigation of temperature dependence and F/OH-effects. *European Journal of Mineralogy* **6**, 53–66.
- Friedman, T. & O'Neil, J. R. (1977). Compilation of stable isotope fractionation factors of geochemical interest. *Data of Geochemistry: US Geological Survey Professional Paper* **440**, 1–12.

- Fritz, P. & Smith, D. G. W. (1970). The isotopic composition of secondary dolomites. *Geochimica et Cosmochimica Acta* **34**, 1161–1173.
- Früh-Green, G. L., Plas, A. & Lécuyer, C. (1996). 14 Petrologic and stable isotope constraints on hydrothermal alteration and serpentinization of the EPR shallow mantle at Hess Deep (site 895). *Proceedings of the Ocean Drilling Program, Scientific Results* **14**, 255–291.
- Ganguly, J. (1982). Thermodynamics of the oxygen isotope fractionation involving plagioclase. *Earth and Planetary Science Letters* **61**, 123–126.
- Garlick, G. D. (1966). Oxygen isotope fractionation in igneous rocks. *Earth and Planetary Science Letters* **1**, 361–368.
- Gautason, B., Chacko, T. & Muehlenbachs, K. (1993). Oxygen isotope partitioning among perovskite (CaTiO₃), cassiterite (SnO₂) and calcite (CaCO₃). *Geological Association of Canada/Mineral Association of Canada Abstracts with Programs, Edmonton, Alberta* **34**.
- Giletti, B. J. (1986). Diffusion effects on oxygen isotope temperatures of slowly cooled igneous and metamorphic rocks. *Earth and Planetary Science Letters* **77**, 218–228.
- Grossman, E. L. & Ku, T.-L. (1986). Oxygen and carbon isotope fractionation in biogenic aragonite: temperature effects. *Chemical Geology: Isotope Geoscience Section* **59**, 59–74.
- Hamann, S. D., Shaw, R. M., Lusk, J. & Batts, B. D. (1984). Isotopic volume differences: The possible influence of pressure on the distribution of sulfur isotopes between sulfide minerals. *Australian Journal of Chemistry* **37**, 1979–1989.
- Hayles, J., Gao, C., Cao, X., Liu, Y. & Bao, H. (2018). Theoretical calibration of the triple oxygen isotope thermometer. *Geochimica et Cosmochimica Acta* **235**, 237–245.
- Heinrich, C. A. (1986). Eclogite facies regional metamorphism of hydrous mafic rocks in the Central Alpine Adula Nappe. *Journal of Petrology* **27**, 123–154.
- Higashino, F., Rubatto, D., Kawakami, T., Bouvier, A. S. & Baumgartner, L. P. (2019). Oxygen isotope speedometry in granulite facies garnet recording fluid/melt–rock interaction (Sør Rondane Mountains, East Antarctica). *Journal of Metamorphic Geology* **37**, 1037–1048.
- Hoffbauer, R., Hoernes, S. & Fiorentini, E. (1994). Oxygen isotope thermometry based on a refined increment method and its application to granulite-grade rocks from Sri Lanka. *Precambrian Research* **66**, 199–220.
- Holland, T. J. B. & Powell, R. (1998). An internally consistent thermodynamic data set for phases of petrological interest. *Journal of Metamorphic Geology* **16**, 309–343.
- Horita, J. (1989). Analytical aspects of stable isotopes in brines. *Chemical Geology: Isotope Geoscience Section* **79**, 107–112.
- Horita, J. (2014). Oxygen and carbon isotope fractionation in the system dolomite–water–CO₂ to elevated temperatures. *Geochimica et Cosmochimica Acta* **129**, 111–124.
- Horita, J. & Clayton, R. N. (2007). Comment on the studies of oxygen isotope fractionation between calcium carbonates and water at low temperatures by Zhou and Zheng (2003; 2005). *Geochimica et Cosmochimica Acta* **71**, 3131–3135.
- Hu, G. & Clayton, R. N. (2003). Oxygen isotope salt effects at high pressure and high temperature and the calibration of oxygen isotope geothermometers. *Geochimica et Cosmochimica Acta* **67**, 3227–3246.
- Javoy, M., Fourcade, S. & Allegre, C. J. (1970). Graphical method for examination of ¹⁸O/¹⁶O fractionations in silicate rocks. *Earth and Planetary Science Letters* **10**, 12–16.
- Joy, H. W. & Libby, W. F. (1960). Size effects among isotopic molecules. *The Journal of Chemical Physics* **33**, 1276–1276.
- Karlssohn, H. R. & Clayton, R. N. (1990). Oxygen isotope fractionation between analcime and water: An experimental study. *Geochimica et Cosmochimica Acta* **54**, 1359–1368.
- Kawabe, I. (1978). Calculation of oxygen isotope fractionation in quartz–water system with special reference to the low temperature fractionation. *Geochimica et Cosmochimica Acta* **42**, 613–621.
- Kendall, C. (1983). Salt effect on oxygen isotope equilibria. *Eos* **64**, 334–335.
- Kieffer, S. W. (1982). Thermodynamics and lattice vibrations of minerals: 5. Applications to phase equilibria, isotopic fractionation, and high-pressure thermodynamic properties. *Reviews of Geophysics* **20**, 827–849.
- Kim, S.-T., Kang, J. O., Yun, S.-T., O’Neil, J. R. & Mucci, A. (2009). Experimental studies of oxygen isotope fractionation between rhodochrosite (MnCO₃) and water at low temperatures. *Geochimica et Cosmochimica Acta* **73**, 4400–4408.
- Kim, S.-T. & O’Neil, J. R. (1997). Equilibrium and nonequilibrium oxygen isotope effects in synthetic carbonates. *Geochimica et Cosmochimica Acta* **61**, 3461–3475.
- Kim, S.-T., O’Neil, J. R., Hillaire-Marcel, C. & Mucci, A. (2007). Oxygen isotope fractionation between synthetic aragonite and water: influence of temperature and Mg²⁺ concentration. *Geochimica et Cosmochimica Acta* **71**, 4704–4715.
- King, E. M., Valley, J. W., Davis, D. W. & Kowallis, B. J. (2001). Empirical determination of oxygen isotope fractionation factors for titanite with respect to zircon and quartz. *Geochimica et Cosmochimica Acta* **65**, 3165–3175.
- Kita, I., Taguchi, S. & Matsubaya, O. (1985). Oxygen isotope fractionation between amorphous silica and water at 34–93 °C. *Nature* **314**, 83–84.
- Kohn, M. J. (1993). Modeling of prograde mineral $\delta^{18}\text{O}$ changes in metamorphic systems. *Contributions to Mineralogy and Petrology* **113**, 249–261.
- Kohn, M. J. & Valley, J. W. (1998a). Effects of cation substitutions in garnet and pyroxene on equilibrium oxygen isotope fractionations. *Journal of Metamorphic Geology* **16**, 625–639.
- Kohn, M. J. & Valley, J. W. (1998b). Obtaining equilibrium oxygen isotope fractionations from rocks: theory and examples. *Contributions to Mineralogy and Petrology* **132**, 209–224.
- Kohn, M. J. & Valley, J. W. (1998c). Oxygen isotope geochemistry of the amphiboles: isotope effects of cation substitutions in minerals. *Geochimica et Cosmochimica Acta* **62**, 1947–1958.
- Kotzer, T. G., Kyser, T. K., King, R. W. & Kerrich, R. (1993). An empirical oxygen-and hydrogen-isotope geothermometer for quartz–tourmaline and tourmaline–water. *Geochimica et Cosmochimica Acta* **57**, 3421–3426.
- Krylov, D. P., Zagnitko, V. N., Hoernes, S., Lugovaja, I. P. & Hoffbauer, R. (2002). Oxygen isotope fractionation between zircon and water: Experimental determination and comparison with quartz–zircon calibrations. *European Journal of Mineralogy* **14**, 849–853.
- Kulla, J. B. (1978). Experimental oxygen isotope fractionation between kaolinite and water. *Short Papers of the 4th International Conference*, pp. 234–235.
- Kusakabe, M. & Robinson, B. W. (1977). Oxygen and sulfur isotope equilibria in the BaSO₄–HSO₄–H₂O system from 110 to 350 °C and applications. *Geochimica et Cosmochimica Acta* **41**, 1033–1040.
- Lacroix, B. & Vennemann, T. (2015). Empirical calibration of the oxygen isotope fractionation between quartz and Fe–Mg–chlorite. *Geochimica et Cosmochimica Acta* **149**, 21–31.
- Lanari, P. & Duesterhoeft, E. (2019). Modeling Metamorphic Rocks Using Equilibrium Thermodynamics and Internally Consistent Databases: Past Achievements, Problems and Perspectives. *Journal of Petrology* **60**, 19–56.

- Leclerc, A. J. & Labeyrie, L. (1987). Temperature dependence of the oxygen isotopic fractionation between diatom silica and water. *Earth and Planetary Science Letters* **84**, 69–74.
- Lichtenstein, U. & Hoernes, S. (1992). Oxygen isotope fractionation between grossular-spessartine garnet and water: an experimental investigation. *European Journal of Mineralogy* **4**, 239–250.
- Lloyd, R. M. (1968). Oxygen isotope behavior in the sulfate-water system. *Journal of Geophysical Research* **73**, 6099–6110.
- Martin, L. A., Rubatto, D., Crépeau, C., Hermann, J., Putlitz, B. & Vitale-Brovarone, A. (2014). Garnet oxygen analysis by SHRIMP-SI: Matrix corrections and application to high-pressure metasomatic rocks from Alpine Corsica. *Chemical Geology* **374**, 25–36.
- Matsuhisa, Y., Goldsmith, J. R. & Clayton, R. N. (1978). Mechanisms of hydrothermal crystallization of quartz at 250 °C and 15 kbar. *Geochimica et Cosmochimica Acta* **42**, 173–182.
- Matsuhisa, Y., Goldsmith, J. R. & Clayton, R. N. (1979). Oxygen isotopic fractionation in the system quartz-albite-anorthite–water. *Geochimica et Cosmochimica Acta* **43**, 1131–1140.
- Matthews, A. (1994). Oxygen isotope geothermometers for metamorphic rocks. *Journal of Metamorphic Geology* **12**, 211–219.
- Matthews, A. & Beckinsale, R. D. (1979). Oxygen isotope equilibrium systematics between quartz and water. *American Mineralogist* **64**, 232–240.
- Matthews, A., Beckinsale, R. D. & Durham, J. J. (1979). Oxygen isotope fractionation between rutile and water and geothermometry of metamorphic eclogites. *Mineralogical Magazine* **43**, 405–413.
- Matthews, A., Goldsmith, J. R. & Clayton, R. N. (1983a). On the mechanisms and kinetics of oxygen isotope exchange in quartz and feldspars at elevated temperatures and pressures. *Geological Society of America Bulletin* **94**, 396–412.
- Matthews, A., Goldsmith, J. R. & Clayton, R. N. (1983b). Oxygen isotope fractionation between zoisite and water. *Geochimica et Cosmochimica Acta* **47**, 645–654.
- Matthews, A., Goldsmith, J. R. & Clayton, R. N. (1983c). Oxygen isotope fractionations involving pyroxenes: the calibration of mineral-pair geothermometers. *Geochimica et Cosmochimica Acta* **47**, 631–644.
- Matthews, A. & Katz, A. (1977). Oxygen isotope fractionation during the dolomitization of calcium carbonate. *Geochimica et Cosmochimica Acta* **41**, 1431–1438.
- Matthews, A., Putlitz, B., Hamiel, Y. & Hervig, R. L. (2003). Volatile transport during the crystallization of anatectic melts: oxygen, boron and hydrogen stable isotope study on the metamorphic complex of Naxos, Greece. *Geochimica et Cosmochimica Acta* **67**, 3145–3163.
- Matthews, A. & Schliestedt, M. (1984). Evolution of the blueschist and greenschist facies rocks of Sifnos, Cyclades, Greece. *Contributions to Mineralogy and Petrology* **88**, 150–163.
- May, P. M. & Murray, K. (2001). Database of chemical reactions designed to achieve thermodynamic consistency automatically. *Journal of Chemical & Engineering Data* **46**, 1035–1040.
- Melchiorre, E. B., Criss, R. E. & Rose, T. P. (2000). Oxygen and carbon isotope study of natural and synthetic azurite. *Economic Geology* **95**, 621–628.
- Melchiorre, E. B., Williams, P. A. & Bevins, R. E. (2001). A low temperature oxygen isotope thermometer for cerussite, with applications at Broken Hill, New South Wales, Australia. *Geochimica et Cosmochimica Acta* **65**, 2527–2533.
- Miron, G. D., Wagner, T., Kulik, D. A. & Heinrich, C. A. (2016). Internally consistent thermodynamic data for aqueous species in the system Na–K–Al–Si–O–H–Cl. *Geochimica et Cosmochimica Acta* **187**, 41–78.
- Miron, G. D., Wagner, T., Kulik, D. A. & Lothenbach, B. (2017). An internally consistent thermodynamic dataset for aqueous species in the system Ca–Mg–Na–K–Al–Si–O–H–Cl to 800 °C and 5 kbar. *American Journal of Science* **317**, 755–806.
- Müller, J. (1995). Oxygen isotopes in iron (III) oxides: a new preparation line; mineral-water fractionation factors and paleoenvironmental considerations. *Isotopes in Environmental and Health Studies* **31**, 301–301.
- Nelder, J. A. & Mead, R. (1965). A simplex method for function minimization. *The Computer Journal* **7**, 308–313.
- Northrop, D. A. & Clayton, R. N. (1966). Oxygen-isotope fractionations in systems containing dolomite. *The Journal of Geology* **74**, 174–196.
- Noto, M. & Kusakabe, M. (1997). An experimental study of oxygen isotope fractionation between wairakite and water. *Geochimica et Cosmochimica Acta* **61**, 2083–2093.
- O’Neil, J. R. (1986). Theoretical and experimental aspects of isotopic fractionation. *Reviews in Mineralogy* **16**, 1–40.
- O’Neil, J. R. & Clayton, R. N. (1964). *Oxygen Isotope Geothermometry. Isotope and Cosmic Chemistry*. Amsterdam: North-Holland Publishing Co., 157–168.
- O’Neil, J. R., Clayton, R. N. & Mayeda, T. K. (1969). Oxygen isotope fractionation in divalent metal carbonates. *The Journal of Chemical Physics* **51**, 5547–5558.
- O’Neil, J. R. & Epstein, S. (1966). Oxygen isotope fractionation in the system dolomite-calcite-carbon dioxide. *Science* **152**, 198–201.
- O’Neil, J. R. & Taylor, H. P. (1967). The oxygen isotope and cation exchange chemistry of feldspars. *American Mineralogist* **52**, 1414–1437.
- O’Neil, J. R. & Taylor, H. P. (1969). Oxygen isotope equilibrium between muscovite and water. *Journal of Geophysical Research* **74**, 6012–6022.
- Page, F. Z., Essene, E. J., Mukasa, S. B. & Valley, J. W. (2014). A garnet–zircon oxygen isotope record of subduction and exhumation fluids from the Franciscan Complex, California. *Journal of Petrology* **55**, 103–131.
- Page, F. Z., Kita, N. T. & Valley, J. W. (2010). Ion microprobe analysis of oxygen isotopes in garnets of complex chemistry. *Chemical Geology* **270**, 9–19.
- Patterson, W. P., Smith, G. R. & Lohmann, K. C. (1993). Continental paleothermometry and seasonality using the isotopic composition of aragonitic otoliths of freshwater fishes. *Climate Change in Continental Isotopic Records* **78**, 191–202.
- Peck, W. H., Valley, J. W. & Graham, C. M. (2003). Slow oxygen diffusion rates in igneous zircons from metamorphic rocks. *American Mineralogist* **88**, 1003–1014.
- Polyakov, V. B. & Kharlashina, N. N. (1994). Effect of pressure on equilibrium isotopic fractionation. *Geochimica et Cosmochimica Acta* **58**, 4739–4750.
- Quinn, R. J., Kitajima, K., Nakashima, D., Spicuzza, M. J. & Valley, J. W. (2017). Oxygen isotope thermometry using quartz inclusions in garnet. *Journal of Metamorphic Geology* **35**, 231–252.
- Richter, R. & Hoernes, S. (1988). The application of the increment method in comparison with experimentally derived and calculated O-isotope fractionations. *Chem. Erde* **48**, 1–18.
- Rosenbaum, J. M. & Matthey, D. (1995). Equilibrium garnet-calcite oxygen isotope fractionation. *Geochimica et Cosmochimica Acta* **59**, 2839–2842.
- Rubatto, D. & Angiboust, S. (2015). Oxygen isotope record of oceanic and high-pressure metasomatism: a P–T–time–fluid

- path for the Monviso eclogites (Italy). *Contributions to Mineralogy and Petrology* **170**, 44.
- Rubatto, D., Putlitz, B., Gauthiez-Putallaz, L., Crépinson, C., Buick, I. S. & Zheng, Y.-F. (2014). Measurement of in-situ oxygen isotope ratios in monazite by SHRIMP ion microprobe: standards, protocols and implications. *Chemical Geology* **380**, 84–96.
- Russell, A. K., Kitajima, K., Strickland, A., Medaris, L. G., Schulze, D. J. & Valley, J. W. (2013). Eclogite-facies fluid infiltration: constraints from $\delta^{18}\text{O}$ zoning in garnet. *Contributions to Mineralogy and Petrology* **165**, 103–116.
- Saccocia, P. J., Seewald, J. S. & Shanks, W. C. III, (1998). Hydrogen and oxygen isotope fractionation between brucite and aqueous NaCl solutions from 250 to 450 °C. *Geochimica et Cosmochimica Acta* **62**, 485–492.
- Savin, S. M. & Epstein, S. (1970). The oxygen and hydrogen isotope geochemistry of clay minerals. *Geochimica et Cosmochimica Acta* **34**, 25–42.
- Savin, S. M. & Lee, M. L. (1988). Isotopic studies of phyllosilicates. *Reviews in Mineralogy and Geochemistry* **19**, 189–223.
- Schmidt, M., Xeflide, S., Botz, R. & Mann, S. (2005). Oxygen isotope fractionation during synthesis of CaMg-carbonate and implications for sedimentary dolomite formation. *Geochimica et Cosmochimica Acta* **69**, 4665–4674.
- Schütze, H. (1980). Der Isotopenindex—eine Inkrementenmethode zur näherungsweise Berechnung von Isotopenaustauschgleichgewichten zwischen kristallinen Substanzen. *Chemie Der Erde* **39**, 321–334.
- Sharp, Z. D. (2017). *Principles of Stable Isotope Geochemistry*, 2nd Edition. University of New Mexico, doi: 10.25844/h9q1-0p82
- Sharp, Z. D. (1995). Oxygen isotope geochemistry of the Al_2SiO_5 polymorphs. *American Journal of Science* **295**, 1058–1076.
- Sharp, Z. D., Gibbons, J. A., Maltsev, O., Atudorei, V., Pack, A., Sengupta, S., Shock, E. L. & Knauth, L. P. (2016). A calibration of the triple oxygen isotope fractionation in the $\text{SiO}_2\text{-H}_2\text{O}$ system and applications to natural samples. *Geochimica et Cosmochimica Acta* **186**, 105–119.
- Sharp, Z. D. & Kirschner, D. L. (1994). Quartz-calcite oxygen isotope thermometry: A calibration based on natural isotopic variations. *Geochimica et Cosmochimica Acta* **58**, 4491–4501.
- Sheppard, S. M. F. & Gilg, H. A. (1996). Stable isotope geochemistry of clay minerals. *Clay Minerals* **31**, 1–24.
- Sheppard, S. M. & Schwarcz, H. P. (1970). Fractionation of carbon and oxygen isotopes and magnesium between coexisting metamorphic calcite and dolomite. *Contributions to Mineralogy and Petrology* **26**, 161–198.
- Shiro, Y. & Sakai, H. (1972). Calculation of the reduced partition function ratios of α -, β -quartz and calcite. *Bulletin of the Chemical Society of Japan* **45**, 2355–2359.
- Smyth, J. R. (1989). Electrostatic characterization of oxygen sites in minerals. *Geochimica et Cosmochimica Acta* **53**, 1101–1110.
- Stern, M. J., Spindel, W. & Monse, E. U. (1968). Temperature dependences of isotope effects. *The Journal of Chemical Physics* **48**, 2908–2919.
- Stoffregen, R. E., Rye, R. O. & Wasserman, M. D. (1994). Experimental studies of alunite: I. ^{18}O - ^{16}O and DH fractionation factors between alunite and water at 250–450 °C. *Geochimica et Cosmochimica Acta* **58**, 903–916.
- Taylor, H. P., Jr & Coleman, R. G. (1968). $\text{O}^{18}/\text{O}^{16}$ ratios of coexisting minerals in glaucophane-bearing metamorphic rocks. *Geological Society of America Bulletin* **79**, 1727–1756.
- Taylor, H. P., Jr, & Epstein, S. (1962). Relationship between $\text{O}^{18}/\text{O}^{16}$ ratios in coexisting minerals of igneous and metamorphic rocks part 1: principles and experimental results. *Geological Society of America Bulletin* **73**, 461–480.
- Tennie, A., Hoffbauer, R. & Hoernes, S. (1998). The oxygen isotope fractionation behaviour of kyanite in experiment and nature. *Contributions to Mineralogy and Petrology* **133**, 346–355.
- Trail, D., Bindeman, I. N., Watson, E. B. & Schmitt, A. K. (2009). Experimental calibration of oxygen isotope fractionation between quartz and zircon. *Geochimica et Cosmochimica Acta* **73**, 7110–7126.
- Truesdell, A. H. (1974). Oxygen isotope activities and concentrations in aqueous salt solutions at elevated temperatures: consequences for isotope geochemistry. *Earth and Planetary Science Letters* **23**, 387–396.
- Urey, H. C. (1947). The thermodynamic properties of isotopic substances. *Journal of the Chemical Society (Resumed)* 562–581.
- Valley, J. W. (1986). Stable isotope geochemistry of metamorphic rocks. *Reviews in Mineralogy and Geochemistry* **16**, 445–489.
- Valley, J. W. (2001). Stable isotope thermometry at high temperatures. *Reviews in Mineralogy and Geochemistry* **43**, 365–413.
- Valley, J. W. (2003). Oxygen isotopes in zircon. *Reviews in Mineralogy and Geochemistry* **53**, 343–385.
- Valley, J. W., Bindeman, I. N. & Peck, W. H. (2003). Empirical calibration of oxygen isotope fractionation in zircon. *Geochimica et Cosmochimica Acta* **67**, 3257–3266.
- Valley, J. W. & Graham, C. M. (1993). Cryptic grain-scale heterogeneity of oxygen isotope ratios in metamorphic magnetite. *Science* **259**, 1729–1733.
- Valley, J. W. & Graham, C. M. (1996). Ion microprobe analysis of oxygen isotope ratios in quartz from Skye granite: healed micro-cracks, fluid flow, and hydrothermal exchange. *Contributions to Mineralogy and Petrology* **124**, 225–234.
- Vasconcelos, C., McKenzie, J. A., Warthmann, R. & Bernasconi, S. M. (2005). Calibration of the $\delta^{18}\text{O}$ paleothermometer for dolomite precipitated in microbial cultures and natural environments. *Geology* **33**, 317–320.
- Vho, A., Lanari, P., Rubatto, D. & Hermann, J. (2020). Tracing fluid transfers in subduction zones: an integrated thermodynamic and $\delta^{18}\text{O}$ fractionation modelling approach. *Solid Earth*, doi:10.5194/se-2019-140
- Vielzeuf, D., Veschambre, M. & Brunet, F. (2005). Oxygen isotope heterogeneities and diffusion profile in composite metamorphic-magmatic garnets from the Pyrenees. *American Mineralogist* **90**, 463–472.
- Vitali, F., Longstaffe, F. J., Bird, M. I. & Caldwell, W. G. E. (2000). Oxygen-isotope fractionation between aluminum-hydroxide phases and water at < 60 °C: Results of decade-long synthesis experiments. *Clays and Clay Minerals* **48**, 230–237.
- Wenner, D. B. & Taylor, H. P. (1971). Temperatures of serpentinization of ultramafic rocks based on $\text{O}^{18}/\text{O}^{16}$ fractionation between coexisting serpentine and magnetite. *Contributions to Mineralogy and Petrology* **32**, 165–185.
- Whitney, D. L. & Evans, B. W. (2010). Abbreviations for names of rock-forming minerals. *American Mineralogist* **95**, 185–187.
- Xu, B.-L. & Zheng, Y.-F. (1999). Experimental studies of oxygen and hydrogen isotope fractionations between precipitated brucite and water at low temperatures. *Geochimica et Cosmochimica Acta* **63**, 2009–2018.
- Yapp, C. J. (1987). Oxygen and hydrogen isotope variations among goethites ($\alpha\text{-FeOOH}$) and the determination of

- paleotemperatures. *Geochimica et Cosmochimica Acta* **51**, 355–364.
- Yapp, C. J. (1990). Oxygen isotopes in iron (III) oxides: 1. Mineral-water fractionation factors. *Chemical Geology* **85**, 329–335.
- Zack, T., Foley, S. F. & Rivers, T. (2002). Equilibrium and disequilibrium trace element partitioning in hydrous eclogites (Trescolmen, Central Alps). *Journal of Petrology* **43**, 1947–1974.
- Zhang, C. L., Horita, J., Cole, D. R., Zhou, J., Lovley, D. R. & Phelps, T. J. (2001). Temperature-dependent oxygen and carbon isotope fractionations of biogenic siderite. *Geochimica et Cosmochimica Acta* **65**, 2257–2271.
- Zhang, L., Liu, J., Chen, Z. & Zhou, H. (1994). Experimental investigations of oxygen isotope fractionation in cassiterite and wolframite. *Economic Geology* **89**, 150–157.
- Zhang, L., Liu, J., Zhou, H. & Chen, Z. (1989). Oxygen isotope fractionation in the quartz-water-salt system. *Economic Geology* **84**, 1643–1650.
- Zheng, Y.-F. (1991). Calculation of oxygen isotope fractionation in metal oxides. *Geochimica et Cosmochimica Acta* **55**, 2299–2307.
- Zheng, Y.-F. (1992). Oxygen isotope fractionation in wolframite. *European Journal of Mineralogy* **4**, 1331–1336.
- Zheng, Y.-F. (1993a). Calculation of oxygen isotope fractionation in anhydrous silicate minerals. *Geochimica et Cosmochimica Acta* **57**, 3199–1091.
- Zheng, Y.-F. (1993b). Calculation of oxygen isotope fractionation in hydroxyl-bearing silicates. *Earth and Planetary Science Letters* **120**, 247–263.
- Zheng, Y.-F. (1993c). Oxygen isotope fractionation in SiO_2 and Al_2SiO_5 polymorphs: effect of crystal structure. *European Journal of Mineralogy* **5**, 651–658.
- Zheng, Y.-F. (1996). Oxygen isotope fractionations involving apatites: application to paleotemperature determination. *Chemical Geology* **127**, 177–187.
- Zheng, Y.-F. (1998). Oxygen isotope fractionation between hydroxide minerals and water. *Physics and Chemistry of Minerals* **25**, 213–221.
- Zheng, Y.-F. (1999). Oxygen isotope fractionation in carbonate and sulfate minerals. *Geochemical Journal* **33**, 109–126.
- Zheng, Y.-F. (2016). Oxygen isotope fractionation in phosphates: the role of dissolved complex anions in isotope exchange. *Isotopes in Environmental and Health Studies* **52**, 47–60.
- Zheng, Y.-F. & Böttcher, M. E. (2016). Oxygen isotope fractionation in double carbonates. *Isotopes in Environmental and Health Studies* **52**, 29–46.
- Zheng, Y.-F., Metz, P., Satir, M. & Sharp, Z. D. (1994). An experimental calibration of oxygen isotope fractionation between calcite and forsterite in the presence of a CO_2 - H_2O fluid. *Chemical Geology* **116**, 17–27.
- Zheng, Y.-F., Wang, Z.-R., Li, S.-G. & Zhao, Z.-F. (2002). Oxygen isotope equilibrium between eclogite minerals and its constraints on mineral Sm-Nd chronometer. *Geochimica et Cosmochimica Acta* **66**, 625–634.
- Zhou, G.-T. & Zheng, Y.-F. (2003). An experimental study of oxygen isotope fractionation between inorganically precipitated aragonite and water at low temperatures. *Geochimica et Cosmochimica Acta* **67**, 387–399.
- Zhou, G.-T. & Zheng, Y.-F. (2005). Effect of polymorphic transition on oxygen isotope fractionation between aragonite, calcite, and water: a low-temperature experimental study. *American Mineralogist* **90**, 1121–1130.

